



SMOS L1 Processor Prototype Phase 3

SMOS L1 Processor Prototype Phase 3

Sun Self-estimation Algorithm **(SMOSP3-UPC-TN-0002 v 1.0)**

Adriano Camps
Mercé Vall·llossera
F. Torres
I. Corbella
N. Duffo

UNIVERSITAT POLITÈCNICA DE CATALUNYA



CONTENTS

1	Scope and objectives	1
2	Introduction: Review of Sun Self-Estimation and Cancellation Algorithms	1
3	Solving the “Singularity” Problem.....	3
3.1	The Sun as a Point Source	3
3.2	The Sun as a Finite Disk.....	4
4	Accounting for the Cross-polar Antenna Patterns.....	6
5	SEPS Simulations	9
6	Conclusions	11
7	References	12
8	Appendixces	13

1 Scope and objectives

This technical note is devoted to the study of the Sun Self-estimation algorithm and the apparent “singularity” that appears when the Sun is 90° (or very close to) away from the array boresight.

In this Technical Note, we analyze the origin of such “singularity”, we demonstrate that it is a mathematical artifact, and propose an closed-form expression for the Sun visibilities to be included in the SMOS End-to-end Performance Simulator (SEPS).

Finally the appropriate modifications of the SEPS functions are provided.

2 Introduction: Review of Sun Self-Estimation and Cancellation Algorithms

Since the Sun is probably the strongest source of contamination, it is highly variable, and it appears in nearly 97% of the snapshots to be acquired by SMOS in [1] an algorithm was proposed to estimate the Sun brightness temperature from the data itself and compensate it from the measured visibilities. The procedure is reviewed here for convenience before actually reviewing the “singularity” problem:

- First a “raw” brightness temperature image is obtained by taking the inverse hexagonal Fourier transform of:

$$\hat{T}_B^{pq} = \mathbf{F}^{-1} \left[V^{pq}(u, v) - V_R^{pq}(u, v) \right], \quad (1)$$

being $V_R^{pq}(u, v)$ the auxiliary visibilities associated to the receivers’ physical temperature in the Corbella equation. Since the Sun is such a bright source it appears as a very bright pixel. Its location in the $(\xi_{Sun,dir}, \eta_{Sun,dir})$ plane can be inferred from it, or it can be computed from the date and the platform position and attitude, whichever is more accurate (it actually depends on the size of the (ξ, η) grid used).

- Second, the instrument’s response for a 1 K amplitude point-source is computed in the direction of the pixel corresponding to the Sun direction (actually an alias of the Sun) in eqn. (1):

$$\hat{T}_{Sun,dir}^{pq} = \mathbf{F}^{-1} \left[\bar{V}_{Sun,dir}^{pq}(u, v) \right]. \quad (2a)$$

$$\begin{aligned} \overline{V}_{Sun,dir}^{pq} \stackrel{\Delta}{=} & \frac{1}{\sqrt{\Omega_1 \Omega_2}} \iint_{\xi^2 + \eta^2 \leq 1} \frac{1}{\sqrt{1 - \xi_{Sun,dir}^2 - \eta_{Sun,dir}^2}} R_{p1}(\xi, \eta) R_{q2}^*(\xi, \eta) \hat{r}_{12} \left(-\frac{u_{12} \xi_{Sun,dir} + v_{12} \eta_{Sun,dir} + w_{12} \sqrt{1 - \xi_{Sun,dir}^2 - \eta_{Sun,dir}^2}}{f_0} \right) \\ & \exp\left(-j2\pi(u_{12} \xi_{Sun,dir} + v_{12} \eta_{Sun,dir} + w_{12} \sqrt{1 - \xi_{Sun,dir}^2 - \eta_{Sun,dir}^2})\right) d\xi d\eta, \end{aligned} \quad (2b)$$

where R_{pn} is the measured copolar antenna pattern at p -polarization of antenna n and \hat{r}_{12} is the fringe-washing function measured aboard by injecting correlated noise at different time lags.

- Third, by subtracting from eqn. (2) an average brightness temperature from the Earth at the Sun's position $(\xi_{Sun,dir}, \eta_{Sun,dir})$, the brightness temperature of Sun can be then estimated as:

$$T_{Sun,dir}^{pq} = \hat{T}_B^{pq}(\xi_{Sun,dir}, \eta_{Sun,dir}) / \hat{T}_{Sun,dir}^{pq}(\xi_{Sun,dir}, \eta_{Sun,dir}). \quad (3)$$

- Finally, the non-normalized visibilities corresponding to the Sun can be estimated from $T_{Sun,dir}^{pq}$ in eqn. (3), the antenna patterns measured on ground, and the fringe-washing function measured aboard:

$$V_{Sun,dir}^{pq}(\mathbf{u}, \mathbf{v}) = T_{Sun,dir}^{pq} \cdot \overline{V}_{Sun,dir}^{pq}(\mathbf{u}, \mathbf{v}). \quad (4)$$

- For the scattered Sun a similar procedure can be applied, but using an appropriate scattering model over the sea or over the land with the necessary auxiliary data (e.g. salinity, temperature, and wind speed, or soil surface temperature, moisture, roughness, and vegetation opacity and albedo):

$$V_{Sun,scatt}^{pq}(\mathbf{u}, \mathbf{v}) = T_{Sun,dir}^{pq} \cdot \overline{V}_{Sun,scatt}^{pq}(\mathbf{u}, \mathbf{v}). \quad (5)$$

However, since the scattered contribution appears always in the aliased region, its impact in the AF-FOV is very small and only due to the spill over from the alias regions into the AF-FOV due to the finite angular resolution [2].

- The self-estimation technique cannot be applied to the Moon since, because of its much lower brightness temperature, there is no clear peak in the brightness temperature images. However, a constant 250 K value can be used [3] and applied. The Moon's contribution to the antenna temperature is negligible, about $250 K (0.5^\circ/60^\circ)^2 = 0.02 K$ if it were located in the antenna boresight.

$$\begin{aligned} \Delta V^{pq}(\mathbf{u}, \mathbf{v}) = & V^{pq}(\mathbf{u}, \mathbf{v}) - V_R^{pq}(\mathbf{u}, \mathbf{v}) - V_{sky}^{pq}(\mathbf{u}, \mathbf{v}) - T_{Earth}^{pq} \overline{V}_{Earth}^{pq}(\mathbf{u}, \mathbf{v}) \\ & - T_{Sun,dir}^{pq} \overline{V}_{Sun,dir}^{pq}(\mathbf{u}, \mathbf{v}) - T_{Sun,dir}^{pq} \overline{V}_{Sun,scatt}^{pq}(\mathbf{u}, \mathbf{v}) \\ & - T_{Moon,dir}^{pq} \overline{V}_{Moon,dir}^{pq}(\mathbf{u}, \mathbf{v}) - T_{Moon,dir}^{pq} \overline{V}_{Moon,scatt}^{pq}(\mathbf{u}, \mathbf{v}) - V_{back}^{pq}(\mathbf{u}, \mathbf{v}), \end{aligned} \quad (6)$$

3 Solving the ‘‘Singularity’’ Problem

3.1 The Sun as a Point Source

The problem comes when trying to compute $V_{Sun,dir}^{pq}(u,v)$, when the Sun position is close to the unit circle ($\xi^2 + \eta^2 = 1$), that is, when it is 90° away from the boresight direction.

$$V_{Sun,dir}^{pq} \stackrel{\Delta}{=} \frac{1}{\sqrt{\Omega_1 \Omega_2}} \iint_{\xi^2 + \eta^2 \leq 1} \frac{T_{B,Sun}(\xi, \eta)}{\sqrt{1 - \xi^2 - \eta^2}} \hat{F}_{n1}^p(\xi, \eta) \hat{F}_{n2}^{q*}(\xi, \eta) \hat{r}_{12} \left(-\frac{u_{12}\xi + v_{12}\eta + w_{12}\sqrt{1 - \xi^2 - \eta^2}}{f_0} \right) \exp(-j2\pi(u_{12}\xi + v_{12}\eta + w_{12}\sqrt{1 - \xi^2 - \eta^2})) d\xi d\eta. \quad (7)$$

Actually, the origin of the ‘‘singularity’’ problem is an error in the way the $T_{B,Sun}$ is expressed in the (ξ, η) coordinate system used to compute eqn. (7), since a delta function in spherical coordinates is cannot be expressed as $\delta(\theta - \theta_0)\delta(\phi - \phi_0)$, but as $\delta(\theta - \theta_0)\delta(\phi - \phi_0) / \sin \theta_0$, which in (ξ, η) coordinates would be $\delta(\xi - \xi_0)\delta(\eta - \eta_0)\sqrt{1 - \xi_0^2 - \eta_0^2}$.

Maybe, the simplest way to show it consists of changing the coordinate system from the (ξ, η) director cosines to the spherical one, which also avoids the ambiguity of the fore and back lobes (same (ξ, η) coordinates for two different directions):

$$\begin{aligned} \xi &= \sin \theta \cos \phi, \\ \eta &= \sin \theta \sin \phi. \end{aligned} \quad (8)$$

Equation (7) then becomes:

$$V_{Sun,dir}^{pq} \stackrel{\Delta}{=} \frac{1}{\sqrt{\Omega_1 \Omega_2}} \int_0^{2\pi} \int_0^\pi T_{B,Sun}(\theta, \phi) \hat{F}_{n1}^p(\theta, \phi) \hat{F}_{n2}^{q*}(\theta, \phi) \hat{r}_{12} \left(-\frac{u_{12} \sin \theta \cos \phi + v_{12} \sin \theta \sin \phi + w_{12} \cos \theta}{f_0} \right) \exp(-j2\pi(u_{12} \sin \theta \cos \phi + v_{12} \sin \theta \sin \phi + w_{12} \cos \theta)) \sin \theta d\theta d\phi. \quad (9)$$

Note that in eqn. (9), the integration over θ has been extended from 0 to π , thus including the possibility that the Sun is in the back of the array. In eqn. (7) to account for the backlobes two integrals had to be computed: one with $+w_{12}$ for $\theta \in [0, \pi/2]$ ($\cos \theta \geq 0$), and a second one $-w_{12}$ for $\theta \in (\pi/2, \pi]$ ($\cos \theta < 0$).

Assuming now that the Sun is a point source (‘‘delta’’ function) at direction $(\theta_{Sun}, \phi_{Sun})$ of value:

$$T_{B,Sun}(\theta, \phi) = \frac{T_{B,Sun0} \Omega_{Sun}}{\sin \theta_{Sun}} \delta(\theta - \theta_{Sun}) \delta(\phi - \phi_{Sun}), \quad (10)$$

eqn. (9) can be readily computed:

$$\begin{aligned} V_{Sun,dir}^{pq} &\stackrel{\Delta}{=} \frac{\Omega_{Sun}}{\sqrt{\Omega_1 \Omega_2}} T_{B,Sun}(\theta_{Sun}, \phi_{Sun}) \hat{F}_{n1}^p(\theta_{Sun}, \phi_{Sun}) \hat{F}_{n2}^{q*}(\theta_{Sun}, \phi_{Sun}) \\ &\hat{f}_{12} \left(-\frac{u_{12} \sin \theta_{Sun} \cos \phi_{Sun} + v_{12} \sin \theta_{Sun} \sin \phi_{Sun} + w_{12} \cos \theta_{Sun}}{f_0} \right) \\ &\exp(-j2\pi(u_{12} \sin \theta_{Sun} \cos \phi_{Sun} + v_{12} \sin \theta_{Sun} \sin \phi_{Sun} + w_{12} \cos \theta_{Sun})). \end{aligned} \quad (11)$$

which is valid for the fore and back lobes of the antennas at any direction, including the $\theta=90^\circ$.

3.2 The Sun as a Finite Disk

When trying to account for the Sun's finite beamwidth, the integration of eqn. (9) is quite cumbersome due to the difficulty to define the integration limits for an arbitrary orientation of the Sun. However, the problem is greatly simplified with an appropriate change of coordinates so that the Sun appears in the direction of a new Z axis. In order to do so, two rotations must be performed:

- From (x, y, z) to (x', y', z') by rotating an angle ϕ_{Sun} around the z axis, and
- From (x', y', z') to (x'', y'', z'') by rotating an angle θ_{Sun} around the y' axis.

These transformations can be expressed as:

$$\begin{bmatrix} x'' \\ y'' \\ z'' \end{bmatrix} = \begin{bmatrix} \cos \theta_{Sun} & 0 & -\sin \theta_{Sun} \\ 0 & 1 & 0 \\ \sin \theta_{Sun} & 0 & \cos \theta_{Sun} \end{bmatrix} \cdot \begin{bmatrix} \cos \phi_{Sun} & \sin \phi_{Sun} & 0 \\ -\sin \phi_{Sun} & \cos \phi_{Sun} & 0 \\ 0 & 0 & 1 \end{bmatrix} \cdot \begin{bmatrix} x \\ y \\ z \end{bmatrix}, \quad (12)$$

and now, the baselines defined in the (x, y, z) coordinate system $(u_{12}, v_{12}, w_{12}) = (x_2 - x_1, y_2 - y_1, z_2 - z_1)/\lambda$, become:

$$\begin{aligned} u''_{12} &= \cos \theta_{Sun} \cos \phi_{Sun} u_{12} + \cos \theta_{Sun} \sin \phi_{Sun} v_{12} - \sin \theta_{Sun} w_{12}, \\ v''_{12} &= -\sin \phi_{Sun} u_{12} + \cos \phi_{Sun} v_{12}, \\ w''_{12} &= \sin \theta_{Sun} \cos \phi_{Sun} u_{12} + \sin \theta_{Sun} \sin \phi_{Sun} v_{12} + \cos \theta_{Sun} w_{12}. \end{aligned} \quad (13)$$

In the (x'', y'', z'') coordinate system, eqn. (9) becomes:

$$\begin{aligned}
 V_{Sun,dir}^{pq} &\stackrel{\Delta}{=} \frac{1}{\sqrt{\Omega_1 \Omega_2}} \int_0^{2\pi} \int_0^{\pi} T_{B,Sun}(\theta'', \phi'') \hat{F}_{n1}^p(\theta'', \phi'') \hat{F}_{n2}^{q*}(\theta'', \phi'') \\
 &\hat{r}_{12} \left(\frac{-u_{12}'' \sin \theta'' \cos \phi'' + v_{12}'' \sin \theta'' \sin \phi'' + w_{12}'' \cos \theta''}{f_0} \right) \\
 &\exp(-j2\pi(u_{12}'' \sin \theta'' \cos \phi'' + v_{12}'' \sin \theta'' \sin \phi'' + w_{12}'' \cos \theta'')) \sin \theta'' d\theta'' d\phi'',
 \end{aligned} \tag{14}$$

and since the Sun extends in $\theta'' = [0, \beta_{Sun}/2]$ and in $\phi'' = [0, 2\pi)$, eqn. (14)

becomes:

$$\begin{aligned}
 V_{Sun,dir}^{pq} &\stackrel{\Delta}{=} \frac{1}{\sqrt{\Omega_1 \Omega_2}} \int_0^{2\pi} \int_0^{\beta_{Sun}/2} T_{B,Sun}(\theta'', \phi'') \hat{F}_{n1}^p(\theta'', \phi'') \hat{F}_{n2}^{q*}(\theta'', \phi'') \\
 &\hat{r}_{12} \left(\frac{-u_{12}'' \sin \theta'' \cos \phi'' + v_{12}'' \sin \theta'' \sin \phi'' + w_{12}'' \cos \theta''}{f_0} \right) \\
 &\exp(-j2\pi(u_{12}'' \sin \theta'' \cos \phi'' + v_{12}'' \sin \theta'' \sin \phi'' + w_{12}'' \cos \theta'')) \sin \theta'' d\theta'' d\phi''.
 \end{aligned} \tag{15}$$

In order to evaluate analytically eqn. (15) some approximations must be performed. Since $\beta_{Sun}/2 \approx 0.293^\circ$ at L-band (slightly larger than in the optical). The obvious one is to approximate all slowly-varying functions by a constant value and take them outside of the integral:

$$\begin{aligned}
 V_{Sun,dir}^{pq} &\stackrel{\Delta}{=} \frac{1}{\sqrt{\Omega_1 \Omega_2}} T_{B,Sun}(\theta_{Sun}, \phi_{Sun}) \hat{F}_{n1}^p(\theta_{Sun}, \phi_{Sun}) \hat{F}_{n2}^{q*}(\theta_{Sun}, \phi_{Sun}) \\
 &\hat{r}_{12} \left(\frac{-u_{12} \sin \theta_{Sun} \cos \phi_{Sun} + v_{12} \sin \theta_{Sun} \sin \phi_{Sun} + w_{12} \cos \theta_{Sun}}{f_0} \right) \\
 &\int_0^{2\pi} \int_0^{\beta_{Sun}/2} \exp(-j2\pi(u_{12}'' \sin \theta'' \cos \phi'' + v_{12}'' \sin \theta'' \sin \phi'' + w_{12}'' \cos \theta'')) \sin \theta'' d\theta'' d\phi''
 \end{aligned} \tag{16a}$$

$$\begin{aligned}
 &= \frac{1}{\sqrt{\Omega_1 \Omega_2}} T_{B,Sun}(\theta_{Sun}, \phi_{Sun}) \hat{F}_{n1}^p(\theta_{Sun}, \phi_{Sun}) \hat{F}_{n2}^{q*}(\theta_{Sun}, \phi_{Sun}) \\
 &\hat{r}_{12} \left(\frac{-u_{12} \sin \theta_{Sun} \cos \phi_{Sun} + v_{12} \sin \theta_{Sun} \sin \phi_{Sun} + w_{12} \cos \theta_{Sun}}{f_0} \right)
 \end{aligned} \tag{16b}$$

$$\begin{aligned}
 &\int_0^{\beta_{Sun}/2} \exp(-j2\pi w_{12}'' \cos \theta'') \sin \theta'' d\theta'' \int_0^{2\pi} \exp\left(-j2\pi \left(\sqrt{u_{12}''^2 + v_{12}''^2} \sin\left(\phi'' + \arctan\left(\frac{u_{12}''}{v_{12}''}\right)\right)\right) \sin \theta''\right) d\phi'' \\
 &= \frac{1}{\sqrt{\Omega_1 \Omega_2}} T_{B,Sun}(\theta_{Sun}, \phi_{Sun}) \hat{F}_{n1}^p(\theta_{Sun}, \phi_{Sun}) \hat{F}_{n2}^{q*}(\theta_{Sun}, \phi_{Sun}) \\
 &\hat{r}_{12} \left(\frac{-u_{12} \sin \theta_{Sun} \cos \phi_{Sun} + v_{12} \sin \theta_{Sun} \sin \phi_{Sun} + w_{12} \cos \theta_{Sun}}{f_0} \right) \\
 &\int_0^{\beta_{Sun}/2} 2\pi J_0\left(-2\pi \sqrt{u_{12}''^2 + v_{12}''^2} \sin \theta''\right) \exp(-j2\pi w_{12}'' \cos \theta'') \sin \theta'' d\theta''
 \end{aligned} \tag{16c}$$

$$\approx \frac{1}{\sqrt{\Omega_1 \Omega_2}} T_{B,Sun}(\theta_{Sun}, \phi_{Sun}) \hat{F}_{n1}^p(\theta_{Sun}, \phi_{Sun}) \hat{F}_{n2}^{q*}(\theta_{Sun}, \phi_{Sun}) \hat{r}_{12} \left(-\frac{u_{12} \sin \theta_{Sun} \cos \phi_{Sun} + v_{12} \sin \theta_{Sun} \sin \phi_{Sun} + w_{12} \cos \theta_{Sun}}{f_0} \right) \quad (16d)$$

$$2\pi \exp(-j2\pi w_{12}^*) \int_0^{\beta_{Sun}/2} \left\{ \theta^n + \left[j\pi w_{12}^* - \frac{1}{6} - \pi^2 (u_{12}^{*2} + v_{12}^{*2}) \right] \theta^{n2} \right\} d\theta^n$$

$$= \frac{1}{\sqrt{\Omega_1 \Omega_2}} T_{B,Sun}(\theta_{Sun}, \phi_{Sun}) \hat{F}_{n1}^p(\theta_{Sun}, \phi_{Sun}) \hat{F}_{n2}^{q*}(\theta_{Sun}, \phi_{Sun}) \hat{r}_{12} \left(-\frac{u_{12} \sin \theta_{Sun} \cos \phi_{Sun} + v_{12} \sin \theta_{Sun} \sin \phi_{Sun} + w_{12} \cos \theta_{Sun}}{f_0} \right) \quad (16e)$$

$$2\pi \exp(-j2\pi(\sin \theta_{Sun} \cos \phi_{Sun} u_{12} + \sin \theta_{Sun} \sin \phi_{Sun} v_{12} + \cos \theta_{Sun} w_{12})) \left\{ \frac{\beta_{Sun}^2}{2} + \left[j\pi w_{12}^* - \frac{1}{6} - \pi^2 (u_{12}^{*2} + v_{12}^{*2}) \right] \frac{\beta_{Sun}^4}{64} \right\}.$$

And substituting the Sun solid angle in eqn. (20): $\Omega_{Sun} = \frac{\pi}{4} \beta_{Sun}^2$

$$V_{Sun,dir}^{pq} = \frac{\Omega_{Sun}}{\sqrt{\Omega_1 \Omega_2}} T_{B,Sun}(\theta_{Sun}, \phi_{Sun}) \hat{F}_{n1}^p(\theta_{Sun}, \phi_{Sun}) \hat{F}_{n2}^{q*}(\theta_{Sun}, \phi_{Sun}) \hat{r}_{12} \left(-\frac{u_{12} \sin \theta_{Sun} \cos \phi_{Sun} + v_{12} \sin \theta_{Sun} \sin \phi_{Sun} + w_{12} \cos \theta_{Sun}}{f_0} \right) \quad (17)$$

$$\exp(-j2\pi(\sin \theta_{Sun} \cos \phi_{Sun} u_{12} + \sin \theta_{Sun} \sin \phi_{Sun} v_{12} + \cos \theta_{Sun} w_{12})) \left\{ 1 + \left[j\frac{w_{12}^*}{2} - \frac{1}{12\pi} - \frac{\pi}{2} (u_{12}^{*2} + v_{12}^{*2}) \right] \Omega_{Sun} \right\},$$

which is identical to eqn. (11) except for the second term within the brackets “{ }” that accounts for the finite size of the Sun.

4 Accounting for the Cross-polar Antenna Patterns

The expression of the visibility function at xx , yx and yy polarizations including the cross-polar antenna patterns are given by:

$$V^{xx} = \frac{1}{\sqrt{\Omega_1 \Omega_2}} \iint_{\xi^2 + \eta^2 \leq 1} \frac{R_{x1} R_{x2}^* (T_{xx}(\xi, \eta) - T_{rec}) + (R_{x1} C_{x2}^* + C_{x1} R_{x2}^*) T_{yx}(\xi, \eta) + C_{x1} C_{x2}^* (T_{yy}(\xi, \eta) - T_{rec})}{\sqrt{1 - \xi^2 - \eta^2}} \hat{r}_{12} \left(-\frac{u_{12} \xi + v_{12} \eta + w_{12} \sqrt{1 - \xi^2 - \eta^2}}{f_0} \right) \exp(-j2\pi(u_{12} \xi + v_{12} \eta + w_{12} \sqrt{1 - \xi^2 - \eta^2})) d\xi d\eta, \quad (18)$$

$$V^{yy} \stackrel{\Delta}{=} \frac{1}{\sqrt{\Omega_1 \Omega_2}} \iint_{\xi^2 + \eta^2 \leq 1} \frac{C_{y1} C_{y2}^* (T_{xx}(\xi, \eta) - T_{rec}) + (R_{y1} C_{y2}^* + C_{y1} R_{y2}^*) T_{yx}(\xi, \eta) + R_{y1} R_{y2}^* (T_{yy}(\xi, \eta) - T_{rec})}{\sqrt{1 - \xi^2 - \eta^2}} \hat{r}_{12} \left(-\frac{u_{12}\xi + v_{12}\eta + w_{12}\sqrt{1 - \xi^2 - \eta^2}}{f_0} \right) \exp(-j2\pi(u_{12}\xi + v_{12}\eta + w_{12}\sqrt{1 - \xi^2 - \eta^2})) d\xi d\eta, \quad (19)$$

and

$$V^{yx} \stackrel{\Delta}{=} \frac{1}{\sqrt{\Omega_1 \Omega_2}} \iint_{\xi^2 + \eta^2 \leq 1} \frac{C_{y1} R_{x2}^* (T_{xx}(\xi, \eta) - T_{rec}) + (R_{y1} R_{x2}^* + C_{y1} C_{x2}^*) T_{yx}(\xi, \eta) + R_{y1} C_{x2}^* (T_{yy}(\xi, \eta) - T_{rec})}{\sqrt{1 - \xi^2 - \eta^2}} \hat{r}_{12} \left(-\frac{u_{12}\xi + v_{12}\eta + w_{12}\sqrt{1 - \xi^2 - \eta^2}}{f_0} \right) \exp(-j2\pi(u_{12}\xi + v_{12}\eta + w_{12}\sqrt{1 - \xi^2 - \eta^2})) d\xi d\eta, \quad (20)$$

where R_{pn} and C_{pn} are the co- and cross-polar antenna patterns at p -polarization corresponding to the n^{th} antenna.

The terms marked in red correspond to the V_R terms that are subtracted in eqn. (1). Note that this term is zero (does not exist) for the cross-polar polarization (yx , eqn. (20)).

The terms marked in blue are additional terms that are neglected when ignoring the antenna cross-polar patterns. The compensation of these terms requires the knowledge of the brightness temperature of the Sun at xx , yy and yx (complex brightness temperature) polarizations, which is not feasible in a direct way.

A potential solution may be the use of an iterative procedure to estimate the $T_{B, Sun}$ at the different polarizations, neglecting the antenna cross-polar pattern terms in eqns. (18)-(20), and then including these estimates in eqns. (18)-(20) to get a better estimate of the $T_{B, Sun}$.

The accuracy of the iterative procedure described is limited by by: 1) the radiometric noise in the visibility samples, and –more important– 2) the error in the average brightness temperature from the Earth at the Sun's position $(\xi_{Sun, dir}, \eta_{Sun, dir})$ that it is subtracted from eqn. (2a).

A reasonable approximation consists of assuming that $T_{B, Sun}^{xx} = T_{B, Sun}^{yy}$ and that $T_{B, Sun}^{yx} = 0$, although it has to be confirmed from radio-astronomical measurements. If this case, eqns. (18)-(20) applied to the Sun, can be simplified as follows:

$$V^{xx} \stackrel{\Delta}{=} \frac{1}{\sqrt{\Omega_1 \Omega_2}} \iint_{\xi^2 + \eta^2 \leq 1} \frac{(R_{x1} R_{x2}^* + C_{x1} C_{x2}^*) (T_{B,Sun}(\xi, \eta) - T_{rec})}{\sqrt{1 - \xi^2 - \eta^2}} \hat{i}_{12} \left(-\frac{u_{12}\xi + v_{12}\eta + w_{12}\sqrt{1 - \xi^2 - \eta^2}}{f_0} \right) \exp(-j2\pi(u_{12}\xi + v_{12}\eta + w_{12}\sqrt{1 - \xi^2 - \eta^2})) d\xi d\eta, \quad (21)$$

$$V^{yy} \stackrel{\Delta}{=} \frac{1}{\sqrt{\Omega_1 \Omega_2}} \iint_{\xi^2 + \eta^2 \leq 1} \frac{(R_{y1} R_{y2}^* + C_{y1} C_{y2}^*) (T_{B,Sun}(\xi, \eta) - T_{rec})}{\sqrt{1 - \xi^2 - \eta^2}} \hat{i}_{12} \left(-\frac{u_{12}\xi + v_{12}\eta + w_{12}\sqrt{1 - \xi^2 - \eta^2}}{f_0} \right) \exp(-j2\pi(u_{12}\xi + v_{12}\eta + w_{12}\sqrt{1 - \xi^2 - \eta^2})) d\xi d\eta, \quad (22)$$

and

$$V^{yx} \stackrel{\Delta}{=} \frac{1}{\sqrt{\Omega_1 \Omega_2}} \iint_{\xi^2 + \eta^2 \leq 1} \frac{(C_{y1} R_{x2}^* + R_{y1} C_{x2}^*) (T_{B,Sun}(\xi, \eta) - T_{rec})}{\sqrt{1 - \xi^2 - \eta^2}} \hat{i}_{12} \left(-\frac{u_{12}\xi + v_{12}\eta + w_{12}\sqrt{1 - \xi^2 - \eta^2}}{f_0} \right) \exp(-j2\pi(u_{12}\xi + v_{12}\eta + w_{12}\sqrt{1 - \xi^2 - \eta^2})) d\xi d\eta, \quad (23)$$

From which the new visibilities corresponding to the Sun ($V_{Sun,dir}^{pq}$) can be readily computed:

$$\begin{aligned} V_{Sun,dir}^{xx} &\stackrel{\Delta}{=} \frac{1}{\sqrt{\Omega_1 \Omega_2}} \iint_{\xi^2 + \eta^2 \leq 1} \frac{(R_{x1} R_{x2}^* + C_{x1} C_{x2}^*) T_{B,Sun}(\xi, \eta)}{\sqrt{1 - \xi^2 - \eta^2}} \hat{i}_{12} \left(-\frac{u_{12}\xi + v_{12}\eta + w_{12}\sqrt{1 - \xi^2 - \eta^2}}{f_0} \right) \exp(-j2\pi(u_{12}\xi + v_{12}\eta + w_{12}\sqrt{1 - \xi^2 - \eta^2})) d\xi d\eta = \\ &= \frac{\Omega_{Sun}}{\sqrt{\Omega_1 \Omega_2}} T_{B,Sun}(\theta_{Sun}, \phi_{Sun}) [R_{x1}(\theta_{Sun}, \phi_{Sun}) R_{x2}^*(\theta_{Sun}, \phi_{Sun}) + C_{x1}(\theta_{Sun}, \phi_{Sun}) C_{x2}^*(\theta_{Sun}, \phi_{Sun})] \\ &\hat{i}_{12} \left(-\frac{u_{12} \sin \theta_{Sun} \cos \phi_{Sun} + v_{12} \sin \theta_{Sun} \sin \phi_{Sun} + w_{12} \cos \theta_{Sun}}{f_0} \right) \\ &\exp(-j2\pi(\sin \theta_{Sun} \cos \phi_{Sun} u_{12} + \sin \theta_{Sun} \sin \phi_{Sun} v_{12} + \cos \theta_{Sun} w_{12})) \\ &\left\{ 1 + \left[j \frac{w_{12}^*}{2} - \frac{1}{12\pi} - \frac{\pi}{2} (u_{12}^{*2} + v_{12}^{*2}) \right] \Omega_{Sun} \right\}, \end{aligned} \quad (24)$$

$$\begin{aligned} V_{Sun,dir}^{yy} &\stackrel{\Delta}{=} \frac{1}{\sqrt{\Omega_1 \Omega_2}} \iint_{\xi^2 + \eta^2 \leq 1} \frac{(R_{y1} R_{y2}^* + C_{y1} C_{y2}^*) T_{B,Sun}(\xi, \eta)}{\sqrt{1 - \xi^2 - \eta^2}} \hat{i}_{12} \left(-\frac{u_{12}\xi + v_{12}\eta + w_{12}\sqrt{1 - \xi^2 - \eta^2}}{f_0} \right) \exp(-j2\pi(u_{12}\xi + v_{12}\eta + w_{12}\sqrt{1 - \xi^2 - \eta^2})) d\xi d\eta = \\ &= \frac{\Omega_{Sun}}{\sqrt{\Omega_1 \Omega_2}} T_{B,Sun}(\theta_{Sun}, \phi_{Sun}) [R_{y1}(\theta_{Sun}, \phi_{Sun}) R_{y2}^*(\theta_{Sun}, \phi_{Sun}) + C_{y1}(\theta_{Sun}, \phi_{Sun}) C_{y2}^*(\theta_{Sun}, \phi_{Sun})] \\ &\hat{i}_{12} \left(-\frac{u_{12} \sin \theta_{Sun} \cos \phi_{Sun} + v_{12} \sin \theta_{Sun} \sin \phi_{Sun} + w_{12} \cos \theta_{Sun}}{f_0} \right) \\ &\exp(-j2\pi(\sin \theta_{Sun} \cos \phi_{Sun} u_{12} + \sin \theta_{Sun} \sin \phi_{Sun} v_{12} + \cos \theta_{Sun} w_{12})) \\ &\left\{ 1 + \left[j \frac{w_{12}^*}{2} - \frac{1}{12\pi} - \frac{\pi}{2} (u_{12}^{*2} + v_{12}^{*2}) \right] \Omega_{Sun} \right\}, \end{aligned} \quad (25)$$

and

$$\begin{aligned}
 V_{Sun,dir}^{yx} &\stackrel{\Delta}{=} \frac{1}{\sqrt{\Omega_1 \Omega_2}} \iint_{\xi^2 + \eta^2 \leq 1} \frac{(C_{y1} R_{x2}^* + R_{y1} C_{x2}^*) T_{B,Sun}(\xi, \eta)}{\sqrt{1 - \xi^2 - \eta^2}} \hat{r}_{12} \left(-\frac{u_{12}\xi + v_{12}\eta + w_{12}\sqrt{1 - \xi^2 - \eta^2}}{f_0} \right) \\
 &\exp\left(-j2\pi(u_{12}\xi + v_{12}\eta + w_{12}\sqrt{1 - \xi^2 - \eta^2})\right) d\xi d\eta = \\
 &= \frac{\Omega_{Sun}}{\sqrt{\Omega_1 \Omega_2}} T_{B,Sun}(\theta_{Sun}, \phi_{Sun}) \left[C_{y1}(\theta_{Sun}, \phi_{Sun}) R_{x2}^*(\theta_{Sun}, \phi_{Sun}) + R_{y1}(\theta_{Sun}, \phi_{Sun}) C_{x2}^*(\theta_{Sun}, \phi_{Sun}) \right] \quad (26) \\
 &\hat{r}_{12} \left(-\frac{u_{12} \sin \theta_{Sun} \cos \phi_{Sun} + v_{12} \sin \theta_{Sun} \sin \phi_{Sun} + w_{12} \cos \theta_{Sun}}{f_0} \right) \\
 &\exp\left(-j2\pi(\sin \theta_{Sun} \cos \phi_{Sun} u_{12} + \sin \theta_{Sun} \sin \phi_{Sun} v_{12} + \cos \theta_{Sun} w_{12})\right) \\
 &\left\{ 1 + \left[j \frac{w_{12}}{2} - \frac{1}{12\pi} - \frac{\pi}{2} (u_{12}^2 + v_{12}^2) \right] \Omega_{Sun} \right\}.
 \end{aligned}$$

Note that when the cross-polar antenna patterns are included, and the $T_{B,Sun}$ is assumed to be the same at both polarizations, then eqn. (23) is also of the form $T_{B,Sun} - T_r$, as in eqns. (21) and (22), and therefore the whole procedure described in eqns. (1)-(6) can be directly applied.

5 SEPS Simulations

The SMOS End-to-end Performance Simulator has been properly modified so as to account for the changes presented in eqns. (24)-(26), mainly the elimination of the obliquity factor, which does not exist when the integral is performed in spherical coordinates or it cancels when the integral is performed in (ξ, η) if the $T_{B,Sun}(\xi, \eta)$ is properly defined), and the inclusion of the term within brackets “{ }” in eqns. (24)-(26), which is the correction due to the finite size of the Sun’s disk. The inclusion of the cross-polar antenna patterns was already implemented in SEPS, and it has been checked that it was already correct.

The list of functions, and the lines that have been modified is listed in the appendix, indicating the nature of the modification. The function `TSun_Moon_estimator.m` has been reformulated for simplicity.

Simulation results using: 1) SEPS Light (visibility samples & reconstruction using an inverse FFT), 2) normal SEPS (visibility samples computed with a double integral & UPC G-matrix reconstruction), and 3) a mixture of normal SEPS for the visibility samples computation and SEPS Light for the image reconstruction have been tested, including the effects of the Sun (110.000 K, worst case for cancellation due to weak



value), the Moon (250 K), and the antenna backlobes, and turning ON and OFF the Sun Cancellation algorithm for two values of the brightness temperature of the Sun: 100.000 K, a quiet value (used to test the capability to estimate the $T_{B,SUN}$ since it appears with moderate values in the reconstructed T_B image) and 1.000.000 K, a strong value, used to test the capability to suppress the main spot and the tails of the impulse response.

Figures 1-20 present the simulation results (see Appendix 2):

- Figures 1-4: $T_{B, Sun} = 100.000$ K without Sun cancellation algorithm applied
 - Figure 1. Y-polarization: top-left: original TB image, top-right: original image truncated to the fundamental (ξ, η) hexagonal period, bottom-left: retrieved TB image by an ideal system ($F_n = 1$, $\tilde{r} = 1$, and no antenna position errors), and bottom-right: retrieved TB image.
 - Figure 2. Y-polarization: top: error between the TB image retrieved by an ideal system and the original one, and bottom error between the TB retrieved image and the original one.
 - Figure 3. Same as Fig. 1 at X-polarization.
 - Figure 4. Same as Fig. 2 at Y-polarization.
- Figures 5-8 (same as Figs. 1-4): $T_{B, Sun} = 100.000$ K with Sun cancellation algorithm applied. Visibility samples and image reconstruction computed using SEPS Light.
- Figures 9-12 (same as Figs. 1-4): $T_{B, Sun} = 100.000$ K with Sun cancellation algorithm applied. Visibility samples computed using normal SEPS (double integrals) and image reconstruction computed using SEPS Light.
- Figures 13-16 (same as Figs. 1-4): $T_{B, Sun} = 100.000$ K with Sun cancellation algorithm applied. Visibility samples and image reconstruction computed using normal SEPS (double integrals & UPC G-matrix).
- Figures 17-20 (same as Figs. 1-4): $T_{B, Sun} = 1.000.000$ K without Sun cancellation algorithm applied. Visibility samples and image reconstruction computed using SEPS Light.
- Figures 21-24 (same as Figs. 1-4): $T_{B, Sun} = 1.000.000$ K with Sun cancellation algorithm applied. Visibility samples and image reconstruction computed using SEPS Light.

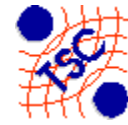
As it can be appreciated:

- The model correctly predicts T_B peaks of the Sun from ~ 80 K to ~ 800 K, as expected from the simple theory ($T_{B,Sun} \propto \Omega_{Sun}/\Omega_{antenna} |F_n|^2$) depending on the Sun brightness temperature, but also on the relative position of the Sun with respect to the antenna boresight (antenna pattern attenuation).
- Simulation results show the improved performance of the Sun cancellation algorithm at both polarizations, both for weak and strong $T_{B,Sun}$ values (100.000-1.000.000 K), although it is expected that it will degrade when the Sun enters through the antenna backlobes, since the amplitude of the T_B peak will be much smaller.

6 Conclusions

The main conclusions of this technical note are summarized hereafter:

- The impact of the Sun has been analyzed, including: ideal point-source case, finite disk size and antenna cross-polarization patterns.
- The “singularity” that appears when formulated in the (ξ, η) domain is originated by an improper formulation of the $T_{B,Sun}(\xi, \eta)$. It can be easily circumvented by formulating the problem in spherical coordinates.
- No averaging is performed between the $T_{B,Sun}$ values at both polarizations as we must from a theoretical point of view in the derivation of eqns. (24)-(26), since these values are not very different (within 10% peak to peak) and in this way, we can compensate for different measurement errors at each polarization.
- Analytical expressions (eqns. (24)-(26)) have been derived for the Sun visibilities including finite angular width of the Sun, antenna cross-polar patterns and fore/back lobes in a single expression.



7 References

- [1] Camps, A., M. Vall-llossera, N. Duffo, M. Zapata, I. Corbella, F. Torres, V. Barrena, Sun Effects In 2D Aperture Synthesis Radiometry Imaging And Their Cancellation, IEEE Transactions on Geoscience and Remote Sensing, Vol. 42 (6), pp. 1161-1167, June 2004
- [2] Camps, A., M. Vall-llossera, N. Reul, F. Torres, N. Duffo, I. Corbella, Impact and Compensation of Diffuse Sun Scattering in 2D Aperture Synthesis Radiometers Imagery, Internacional Geoscience and Remote Sensing Symposium IGARSS 2005, Seoul. Korea, 25-29 July 2005
- [3] Kopal, A., The Moon, ed. Reidel, Dordrecht, 1969

8 Appendix 1

File name	Lines changed	Comment
area_pixel.m		File replaced by two new files area_pixel_sun.m and area_pixel_moon.m to allow for different Sun and Moon solid angles at L-band
mirasvis.m	172, 184, 196, 205, 220, 232, 244, 256, 270, 271, 408, 410, 411, 418, 420, 421, 429, 431, 432	area_pixel_sun & area_pixel_moon are now different to account for the different solid angles subtended by the Sun and the Moon at L-band (at optical frequencies they are the same).
	516-531	computation of some new auxiliary variables needed
	533, 535, 538, 550, 552, 554, 568, 570, 572, 584, 586, 589	invOF term removed and substituted by the term: $\exp(-j2\pi(\sin\theta_{sun}\cos\phi_{sun}u_{12} + \sin\theta_{sun}\sin\phi_{sun}v_{12} + \cos\theta_{sun}w_{12}))$ $\left\{1 + \left[j\frac{w_{12}^*}{2} - \frac{1}{12\pi} - \frac{\pi}{2}(u_{12}^2 + v_{12}^2) \right] \Omega_{sun} \right\}$
mirasvis_fft.m	146, 155, 170, 182, 194, 206, 218, 230, 244, 245	area_pixel_sun & area_pixel_moon are now different to account for the different solid angles subtended by the Sun and the Moon at L-band (at optical frequencies they are the same).
	381, 383, 384, 391, 392, 393, 402, 404, 405, 462, 464, 465, 481, 483, 484, 501, 503, 504, 521, 523, 524	invOF term removed
mirasvis_back.m	98-113	computation of some new auxiliary variables needed
	115, 117, 119, 132, 134, 136, 150, 152, 154	invOF term removed and substituted by the term: $\exp(-j2\pi(\sin\theta_{sun}\cos\phi_{sun}u_{12} + \sin\theta_{sun}\sin\phi_{sun}v_{12} + \cos\theta_{sun}w_{12}))$ $\left\{1 + \left[j\frac{w_{12}^*}{2} - \frac{1}{12\pi} - \frac{\pi}{2}(u_{12}^2 + v_{12}^2) \right] \Omega_{sun} \right\}$
mirasvis_back_fft.m	77, 79, 80, 96, 98, 99, 116, 118, 119, 136, 138, 139	invOF term removed
	88, 107, 147	Error corrected: eee_ref_moon
miras_TA_back.m	94, 95, 96, 103, 104, 105, 113, 114, 115	invOF term removed
miras_auxiliary_visibilities.m	71, 72, 79, 80, 110, 111, 118, 119, 152, 153, 159, 169	invOF term removed
mirasvis_aux.m	148, 150, 152, 183, 185, 187, 219, 221, 223, 252 - 262	invOF term removed
mirasvis_aux_fft.m	114, 116, 117, 158, 160, 161, 204, 206, 207, 243-256	invOF term removed
mirasvis_aux_back.m	141-156	computation of some new auxiliary variables needed
	158, 160, 162, 184, 186, 188, 211, 213, 215	invOF term removed and substituted by the term: $\exp(-j2\pi(\sin\theta_{sun}\cos\phi_{sun}u_{12} + \sin\theta_{sun}\sin\phi_{sun}v_{12} + \cos\theta_{sun}w_{12}))$ $\left\{1 + \left[j\frac{w_{12}^*}{2} - \frac{1}{12\pi} - \frac{\pi}{2}(u_{12}^2 + v_{12}^2) \right] \Omega_{sun} \right\}$
mirasvis_aux_back_fft.m	149, 150, 151, 183, 184, 185, 218, 219, 220, 241-251	invOF term removed
TSun_Moon_estimator.m		function rewritten for simplicity

Appendix 2.

TBSUN = 100.000 K, NO SUN CANCELLATION ALGORITHM APPLIED

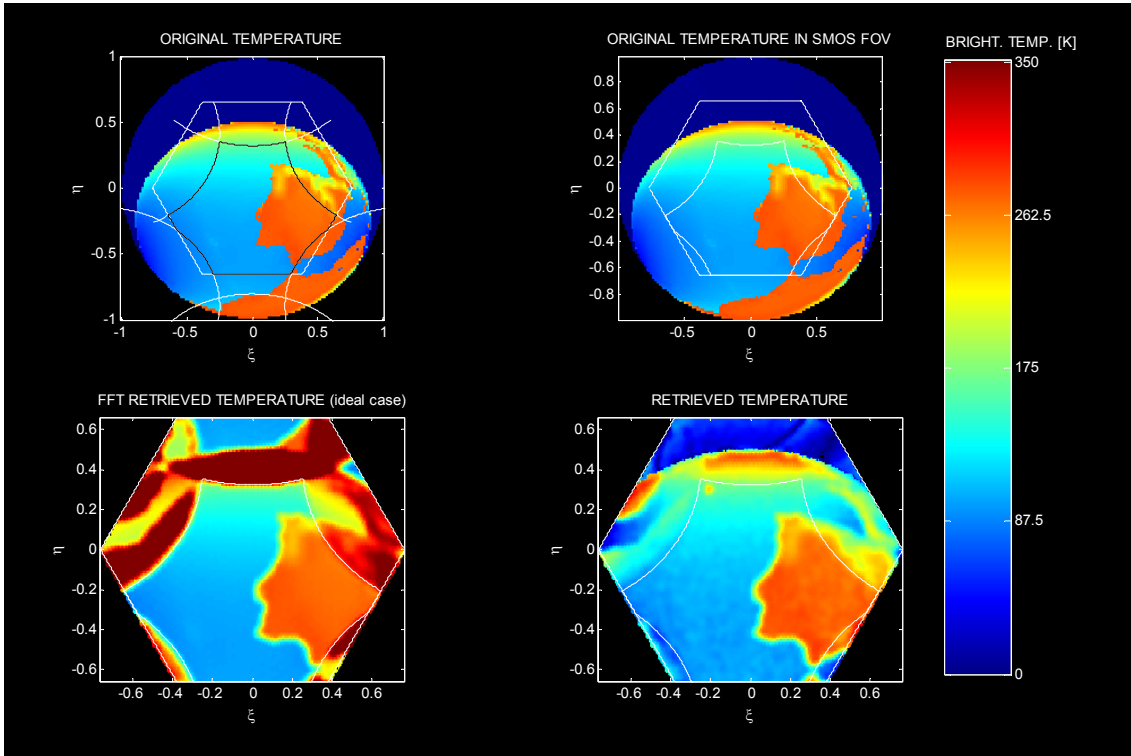


Fig. 1. Y-pol. SEPS Light. No Sun cancellation algorithm applied

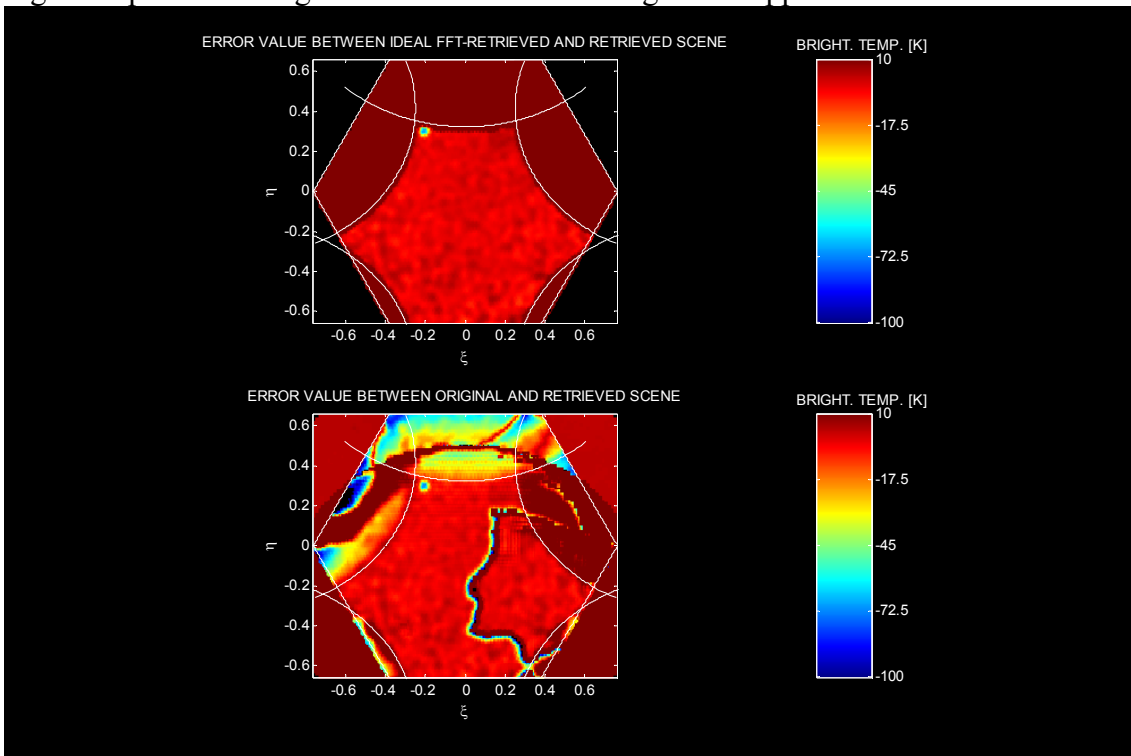


Fig. 2. Y-pol error SEPS Light. No Sun cancellation algorithm applied

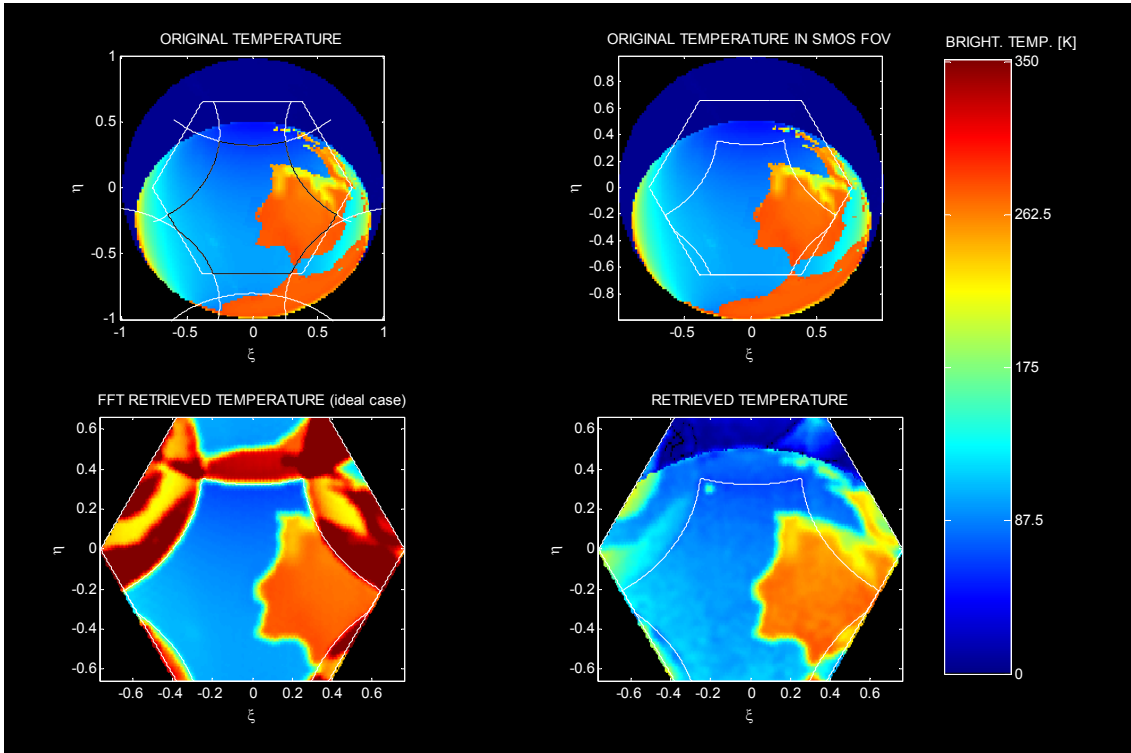


Fig. 3. X-pol SEPS Light. No Sun cancellation algorithm applied

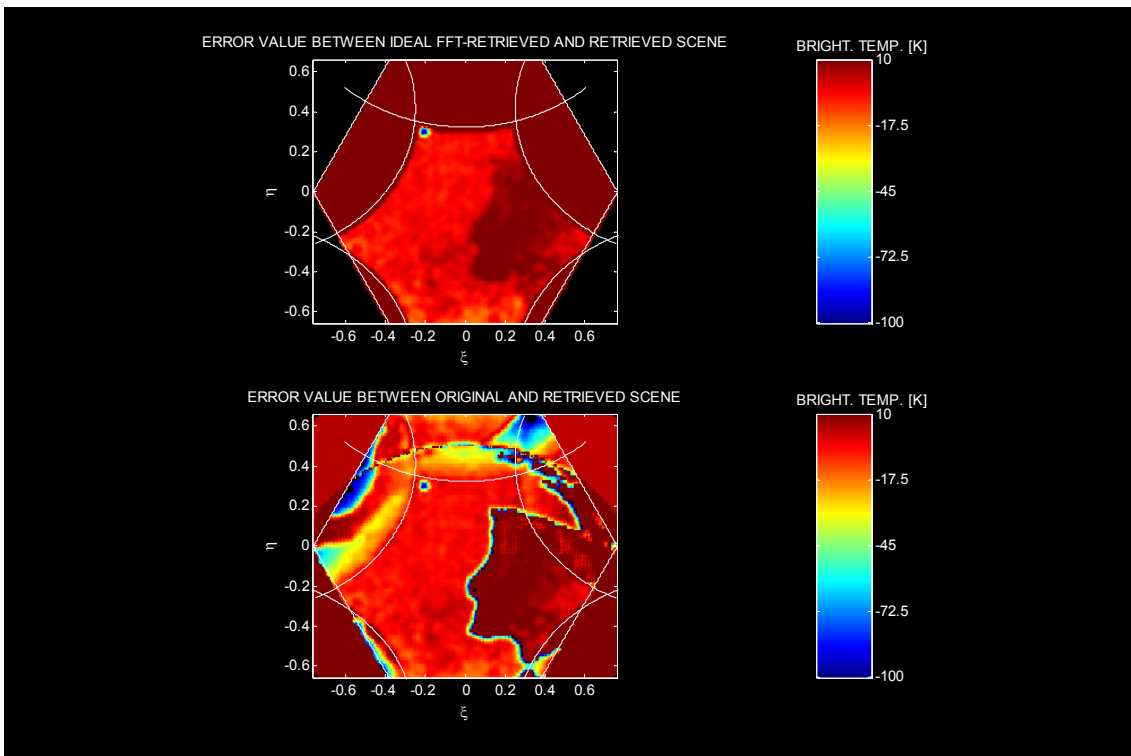


Fig. 4. X-pol error SEPS Light. No Sun cancellation algorithm applied

TBSUN = 1.00.000 K. SUN CANCELLATION ALGORITHM APPLIED:

Estimated TB_SUN at Y-polarization: 112596.4322 Kelvin

Estimated TB_SUN at X-polarization: 100958.8888 Kelvin

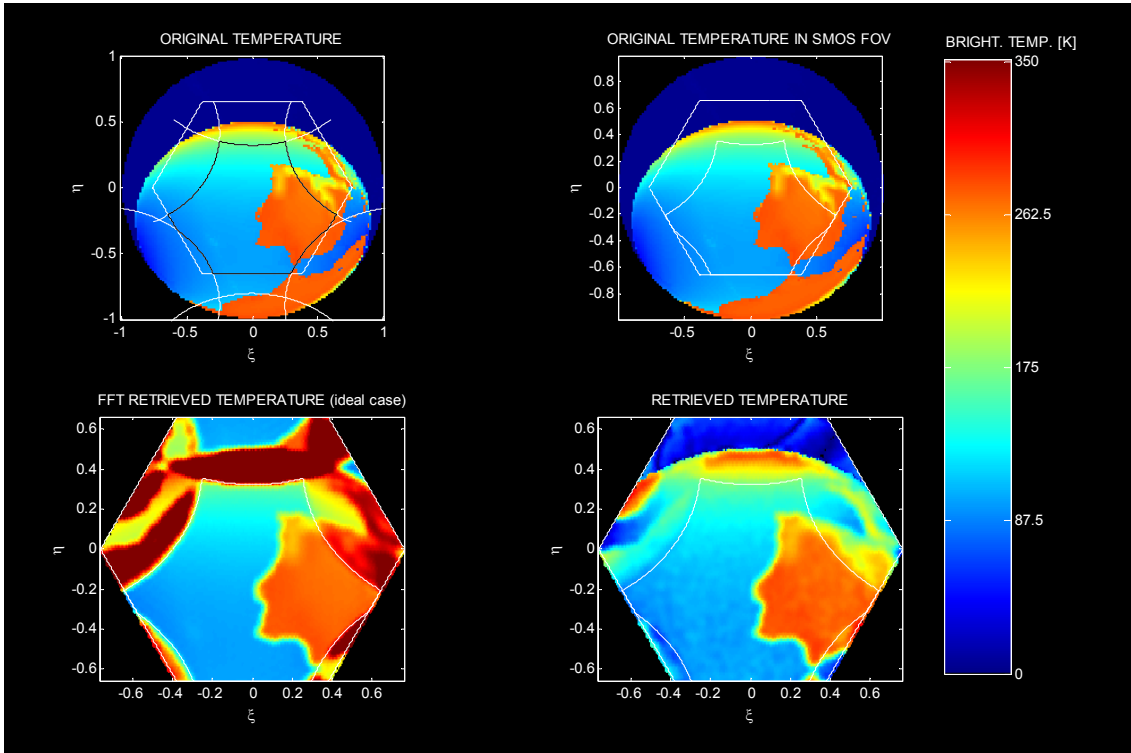


Fig. 5. Y-pol. SEPS Light

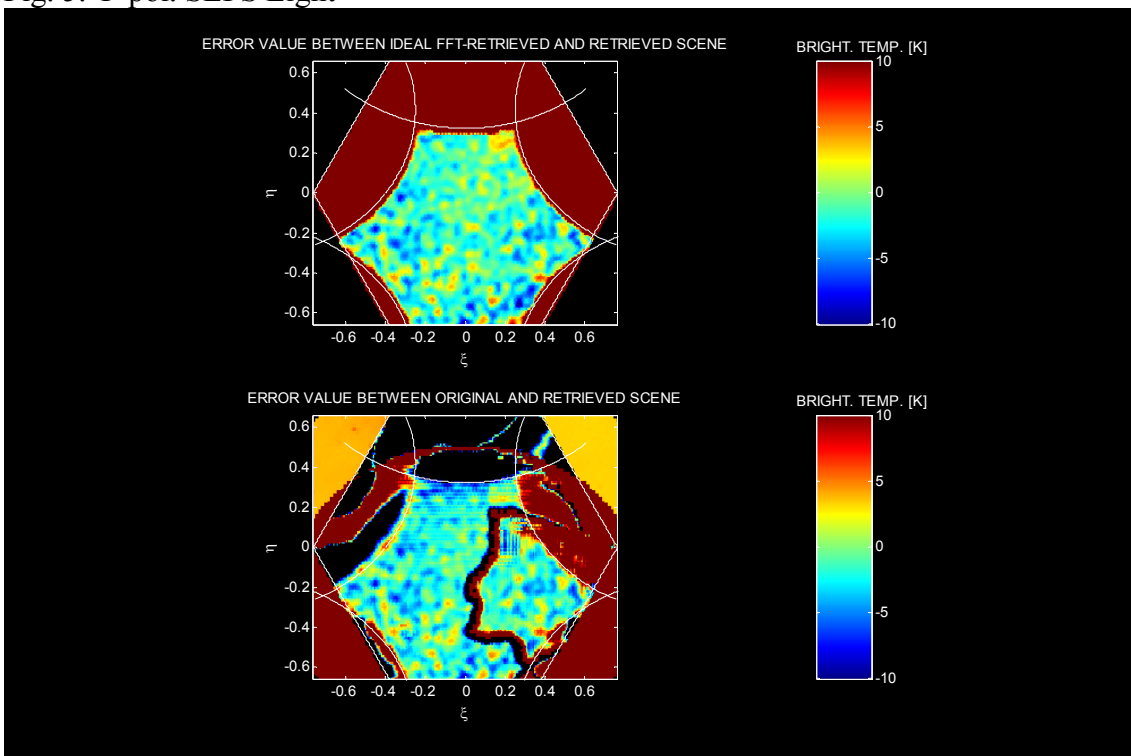


Fig. 6. Y-pol error SEPS Light

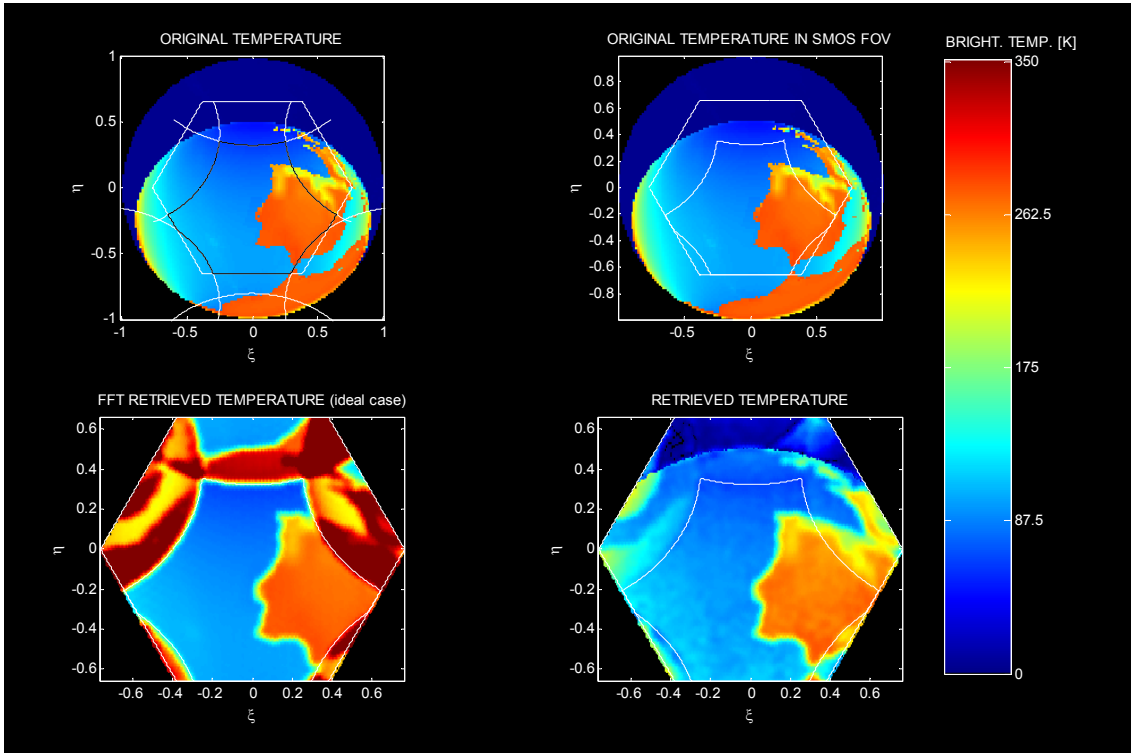


Fig. 7. X-pol SEPS Light

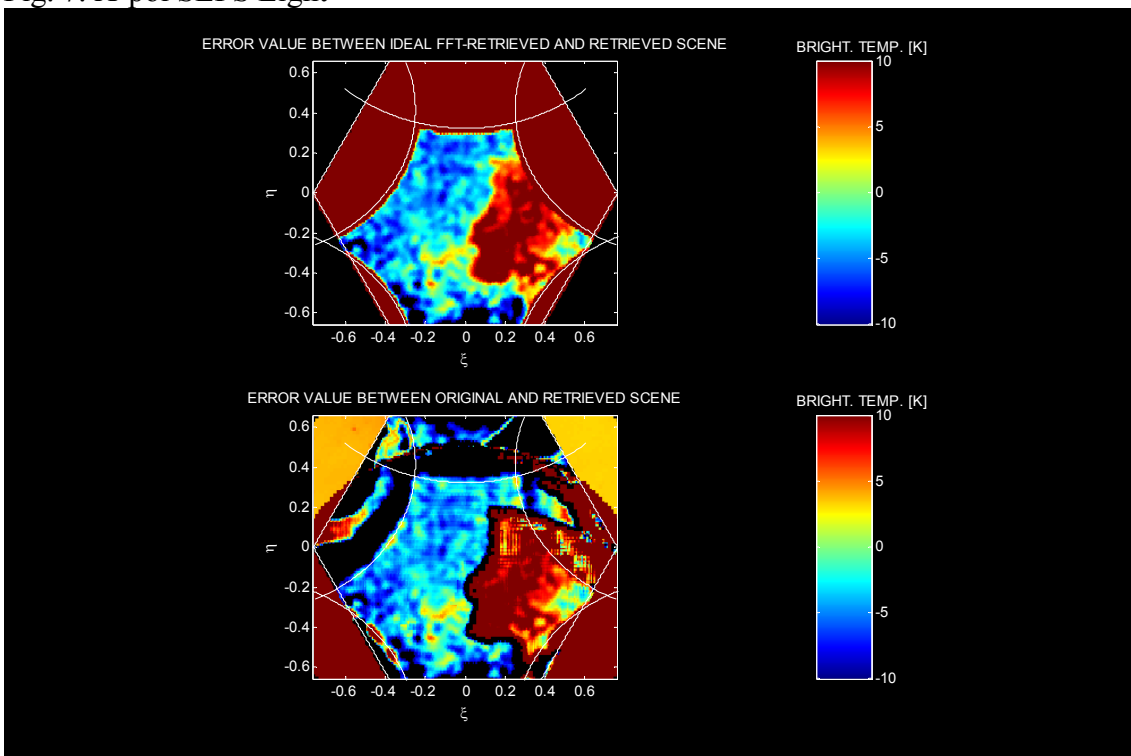


Fig. 8. X-pol error SEPS Light

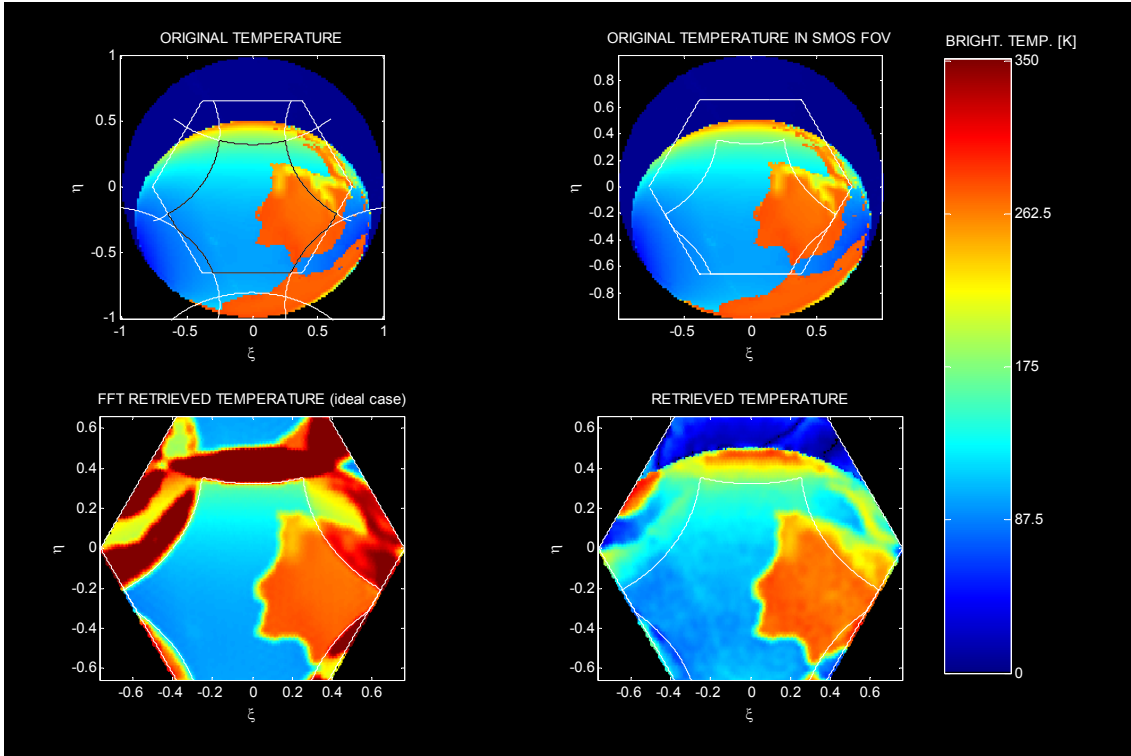


Fig. 9. Y-pol. Visibility generation using normal SEPS, image reconstruction using SEPS Light

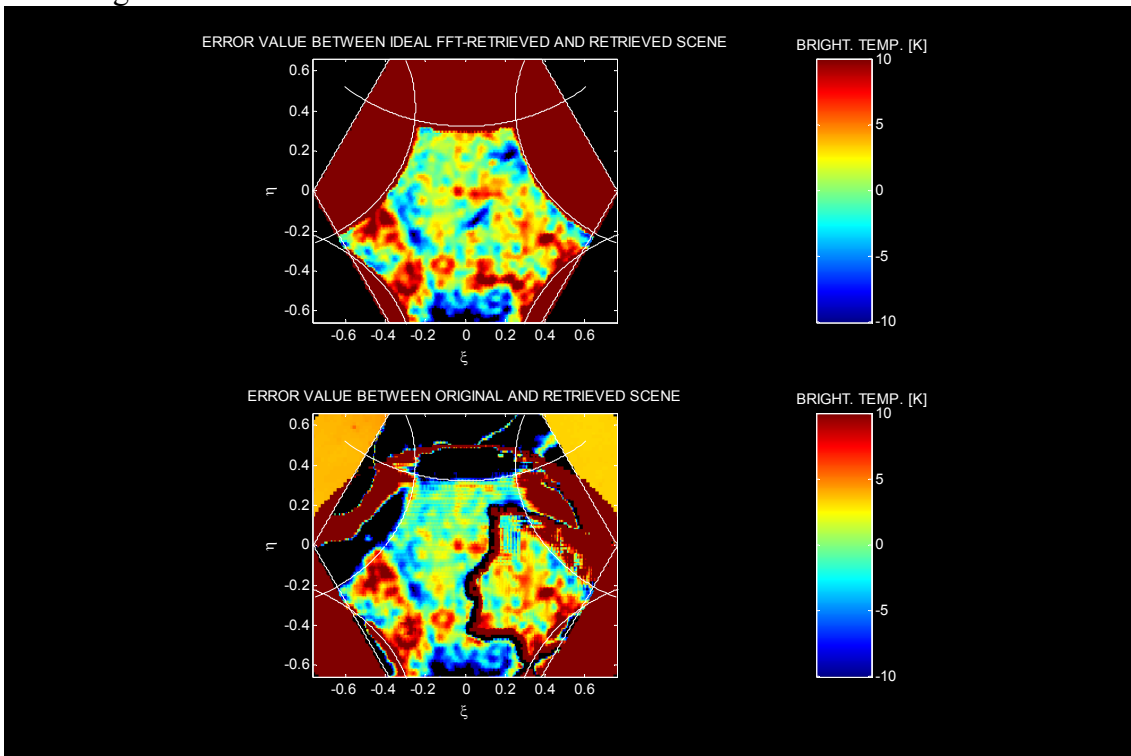


Fig. 10. Y-pol. TB Error. Visibility generation using normal SEPS, image reconstruction using SEPS Light

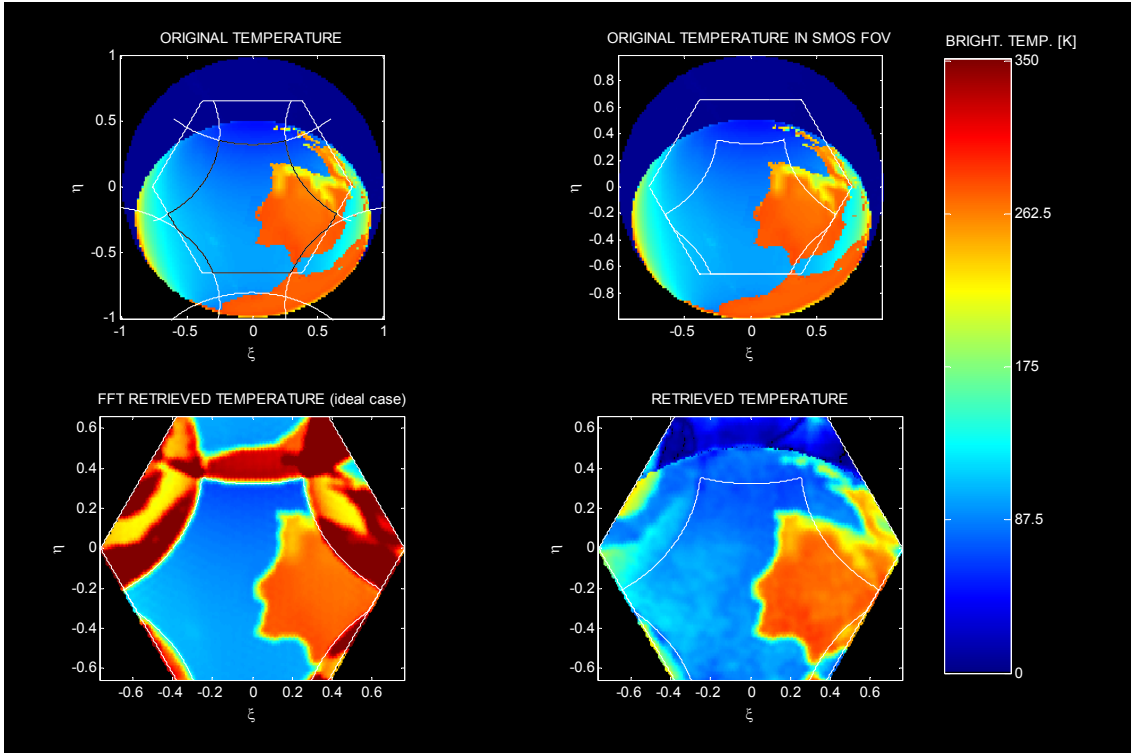


Fig. 11. X-pol. TB. Visibility generation using normal SEPS, image reconstruction using SEPS Light

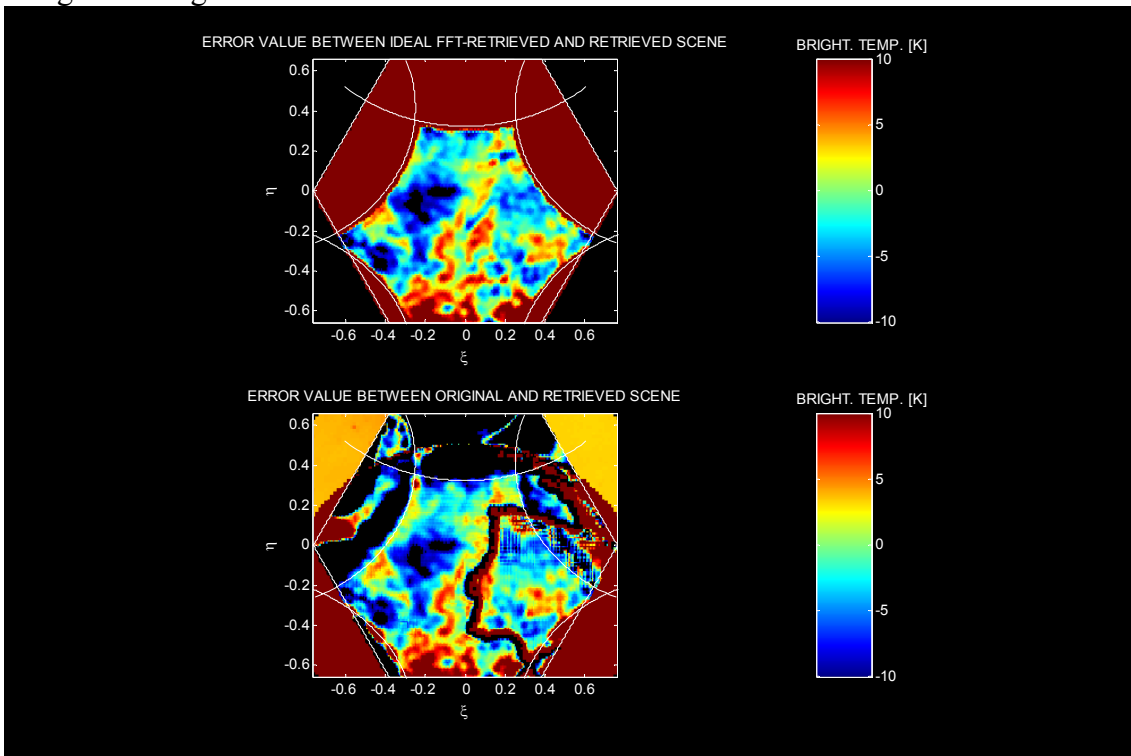


Fig. 12. X-pol. TB Error. Visibility generation using normal SEPS, image reconstruction using SEPS Light

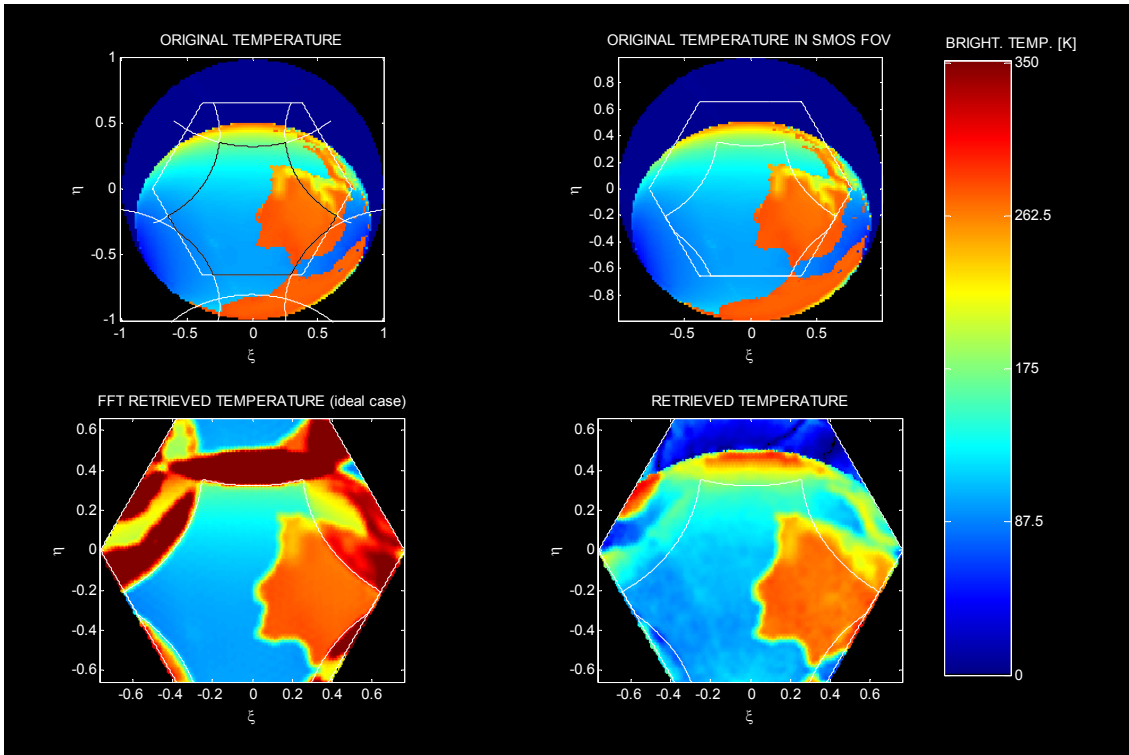


Fig. 13. Y-pol. TB. Visibility generation and image reconstruction using normal SEPS.

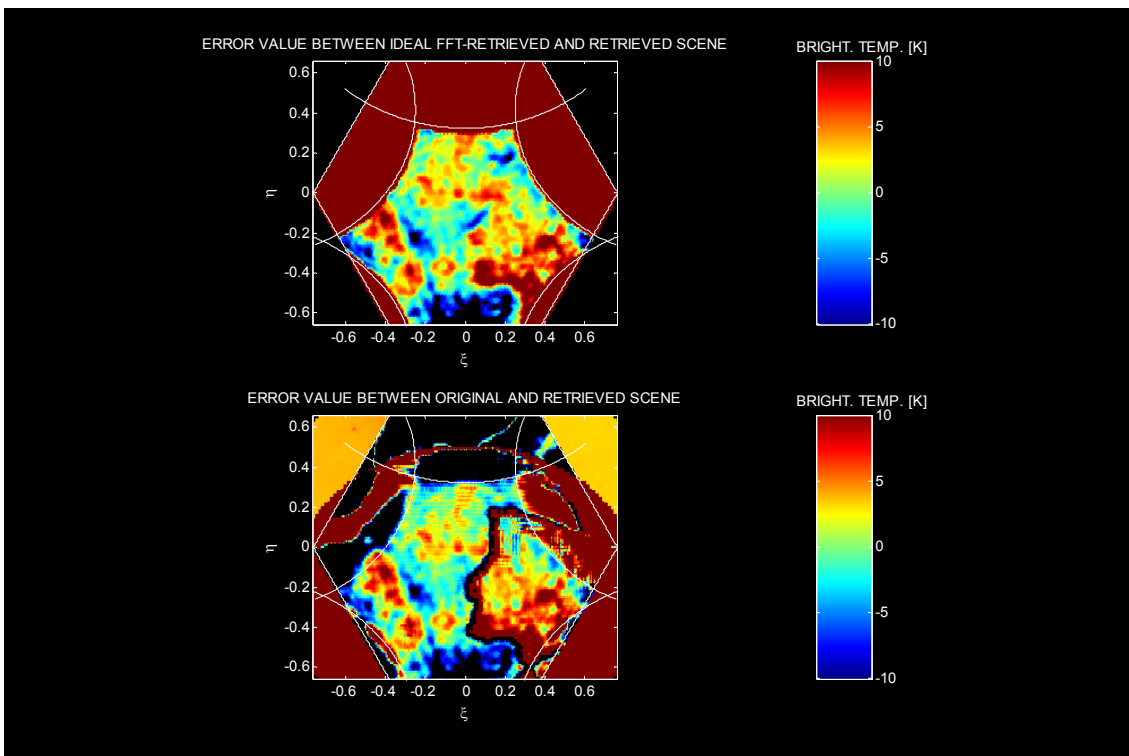


Fig. 14. Y-pol. TB error. Visibility generation and image reconstruction using normal SEPS.

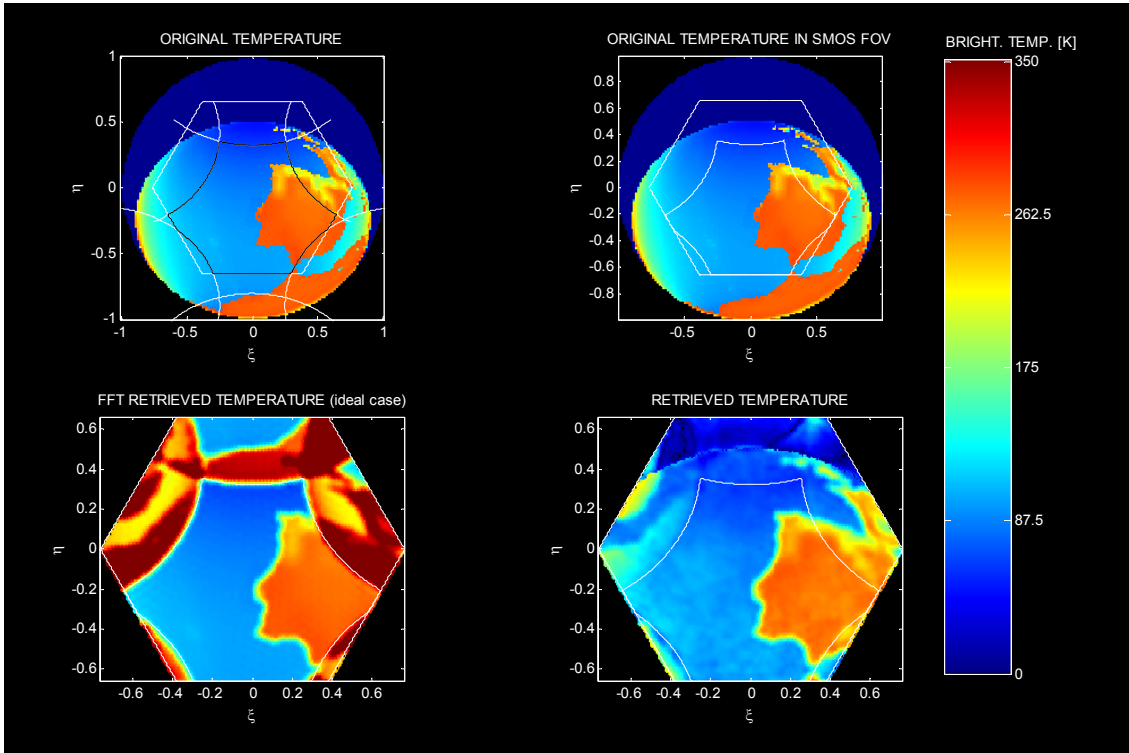


Fig. 15. X-pol. TB. Visibility generation and image reconstruction using normal SEPS.

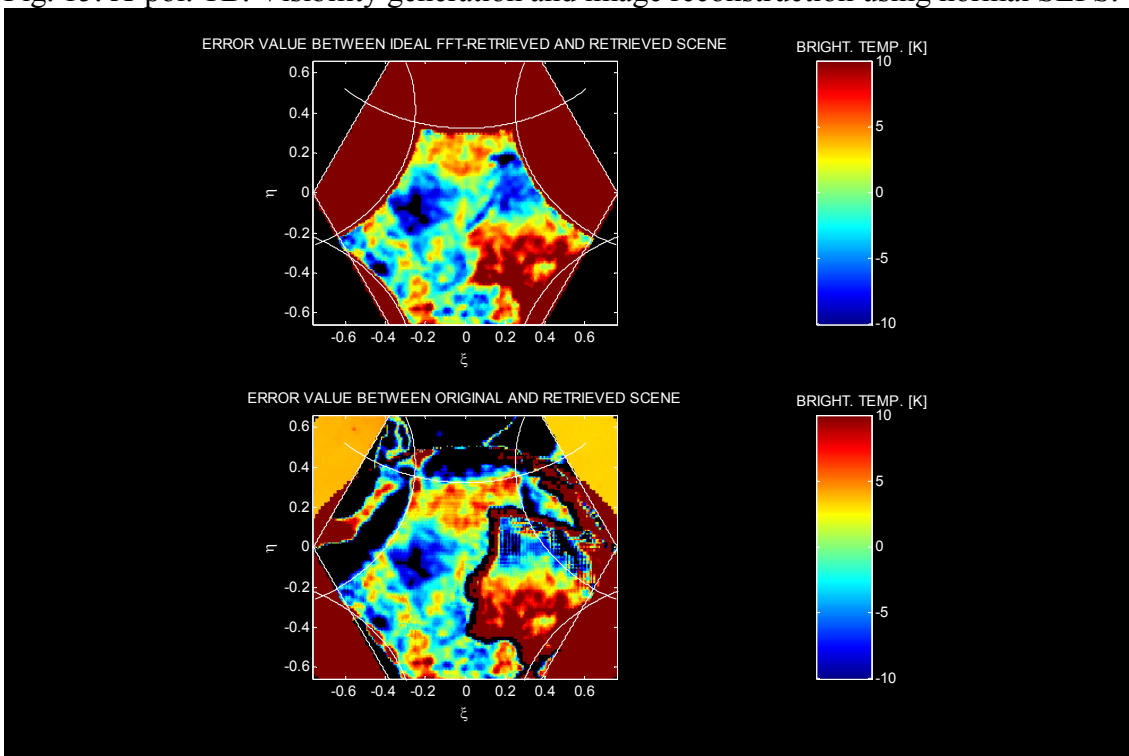


Fig. 16. X-pol. TB error. Visibility generation and image reconstruction using normal SEPS.

TBSUN = 1.000.000 K, NO SUN CANCELLATION ALGORITHM APPLIED

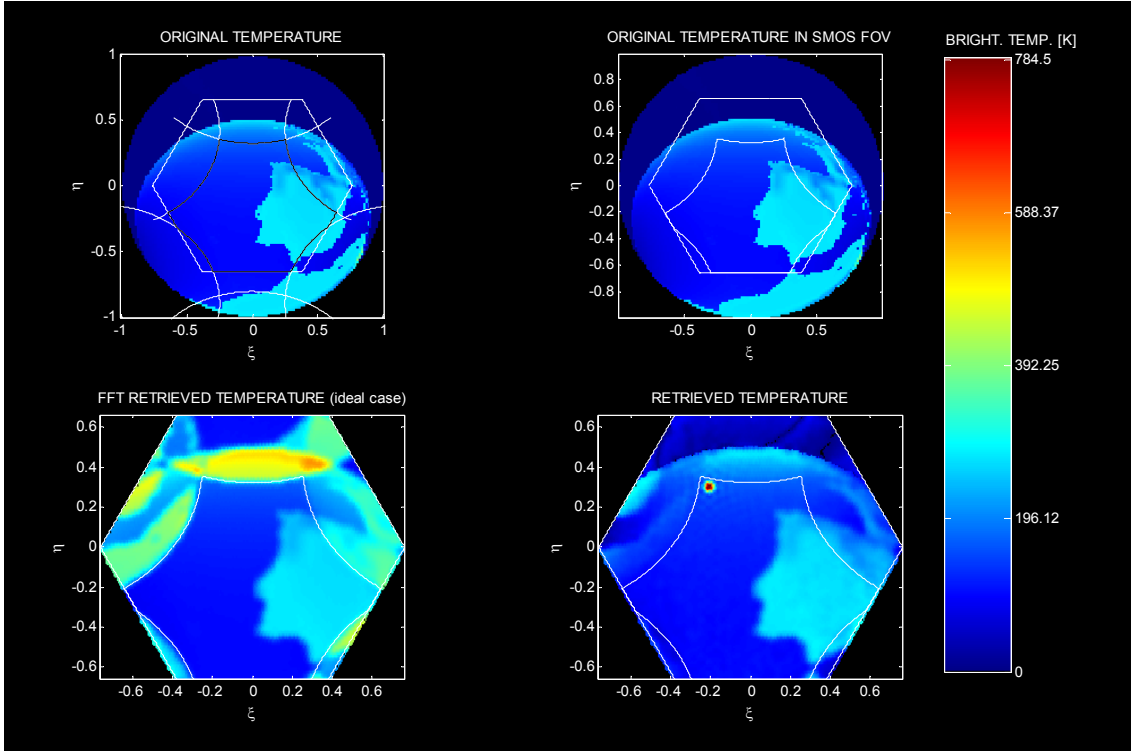


Fig. 17. Y-pol. TB. Visibility generation and image reconstruction using SEPS Light.

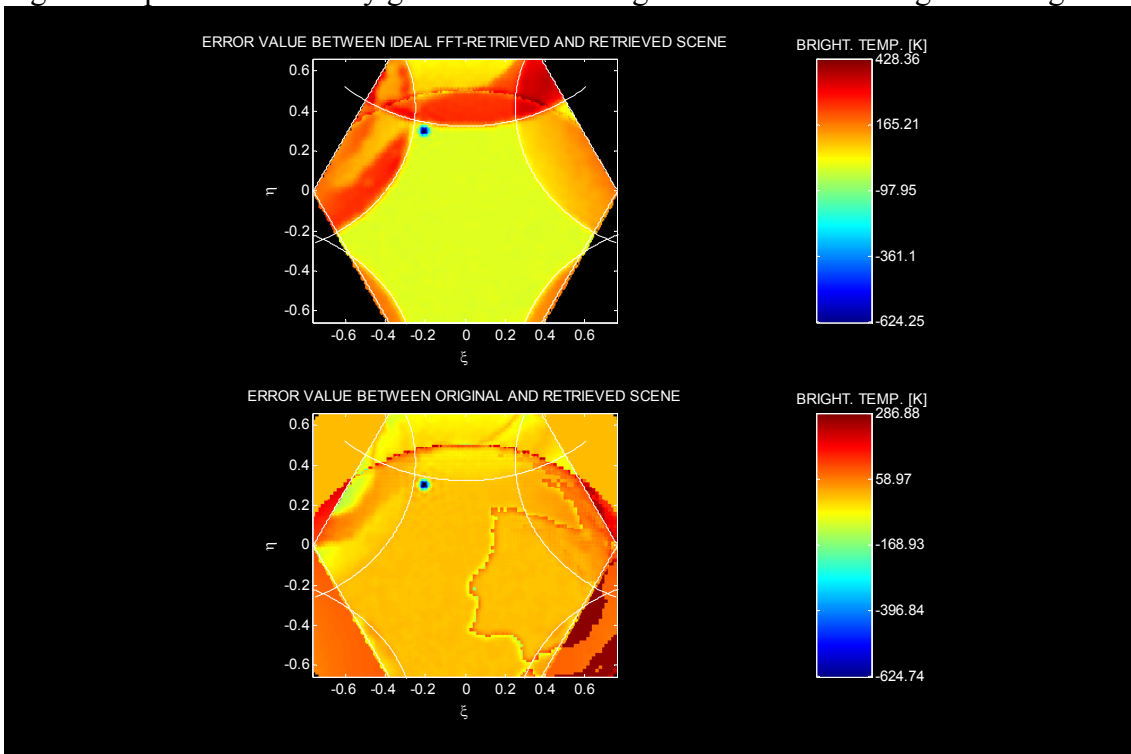


Fig. 18. Y-pol. TB error. Visibility generation and image reconstruction using SEPS Light

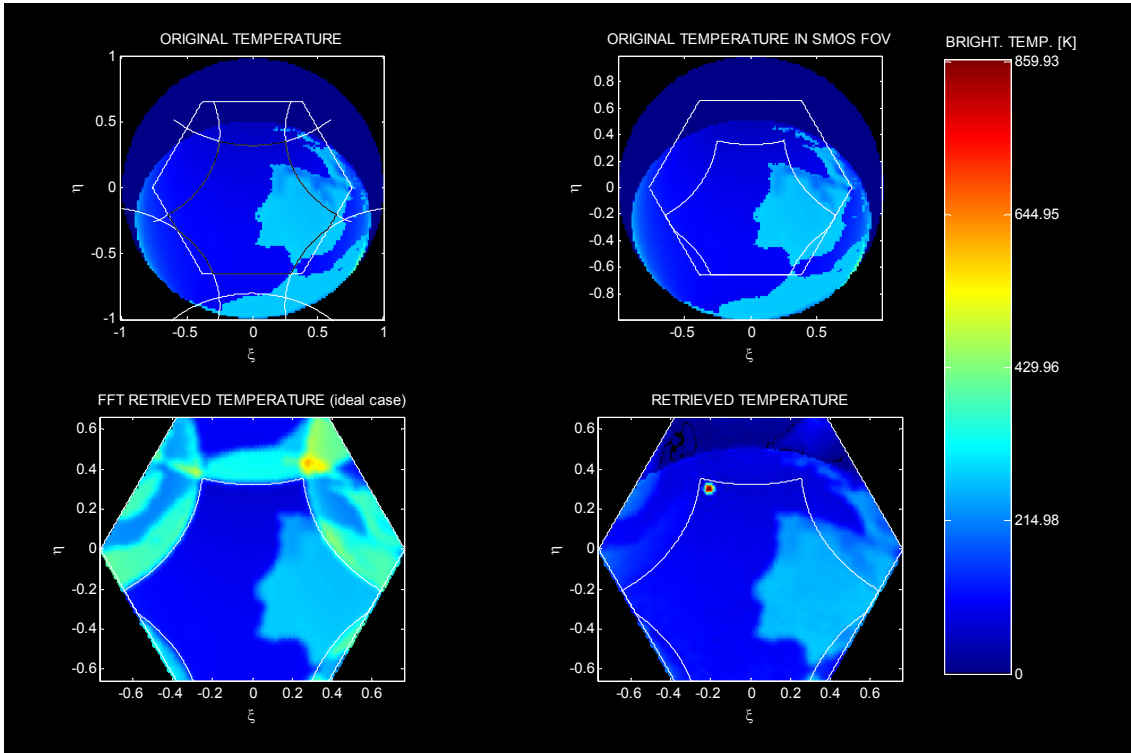


Fig. 19. X-pol. TB. Visibility generation and image reconstruction using SEPS Light

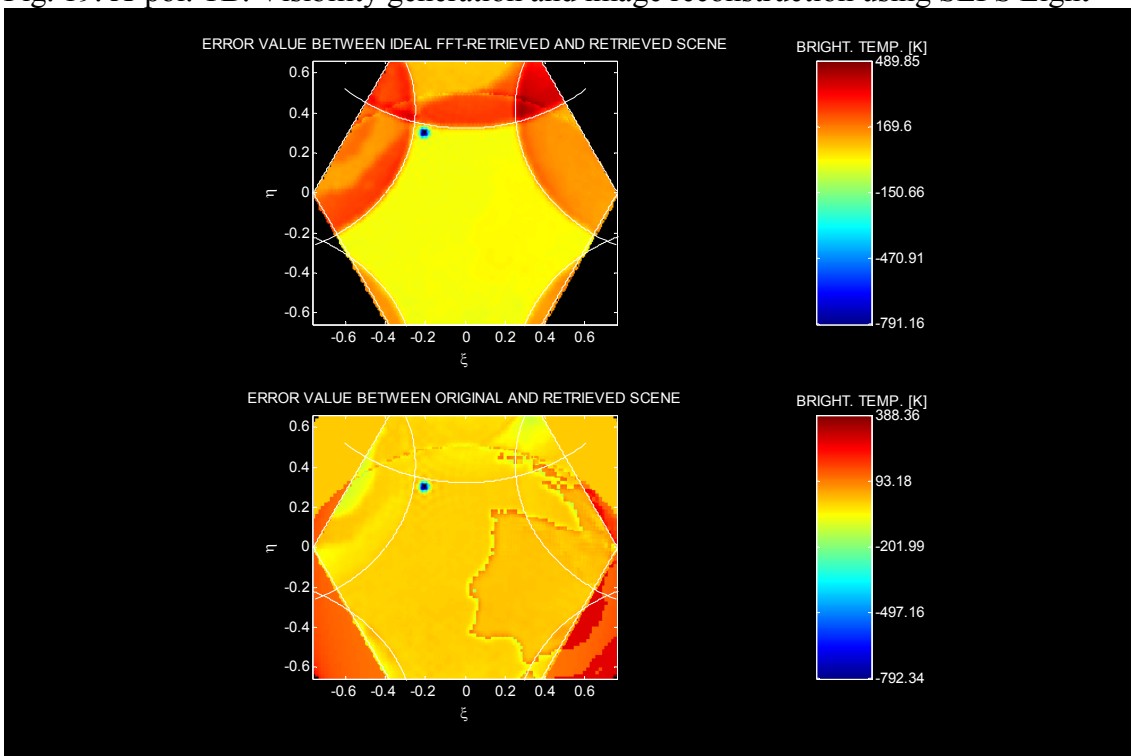


Fig. 20. X-pol. TB error. Visibility generation and image reconstruction using SEPS Light

TBSUN = 1.000.000 K. SUN CANCELLATION ALGORITHM APPLIED:

Estimated TB_SUN at Y-polarization: 996240.5809 Kelvin

Estimated TB_SUN at X-polarization: 920585.0071 Kelvin

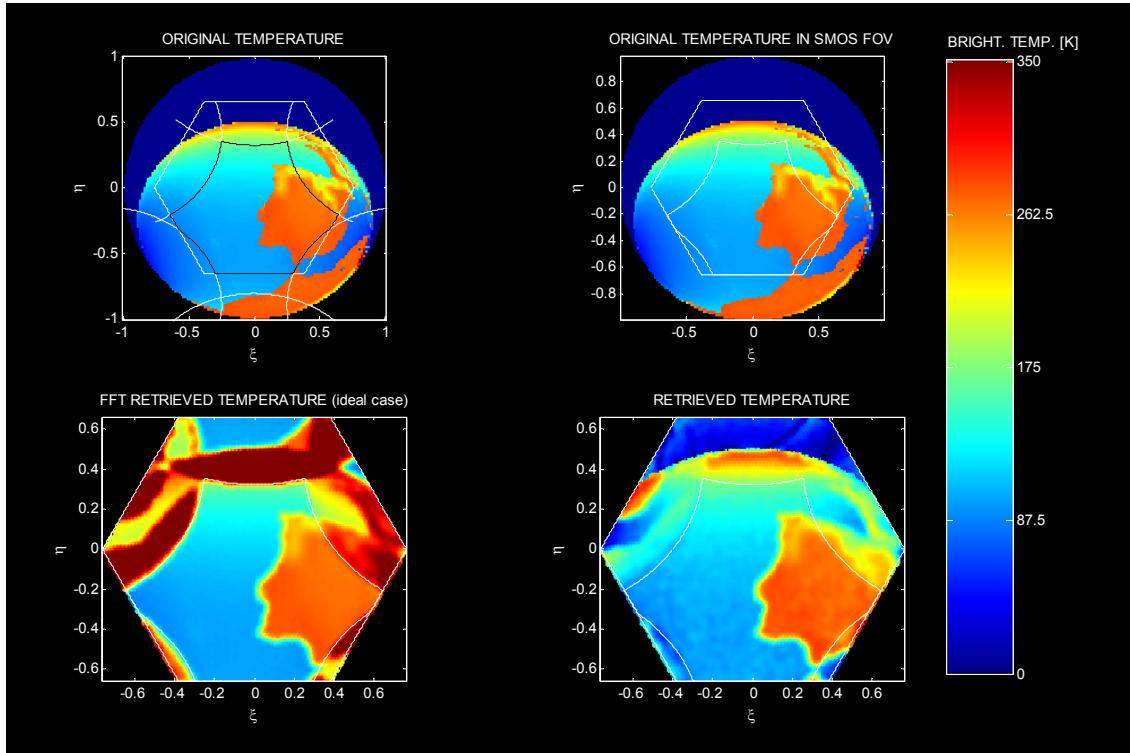


Fig. 21. Y-pol. TB. Visibility generation and image reconstruction using SEPS Light.

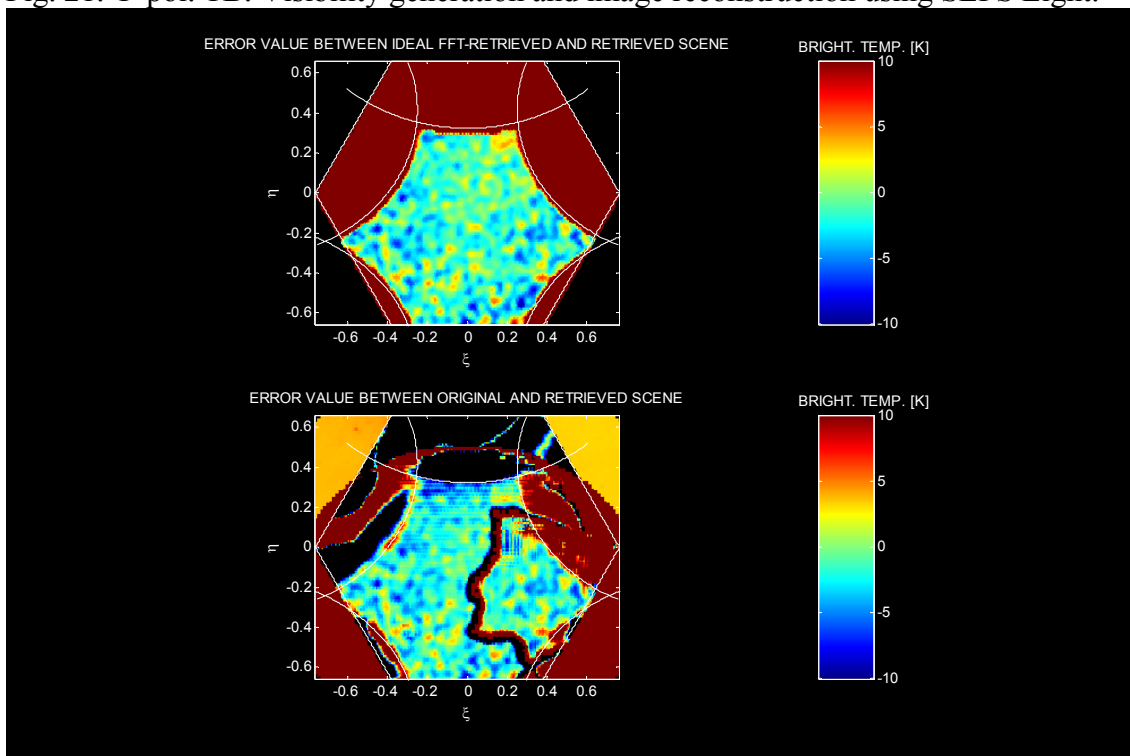


Fig. 21. Y-pol. TB error. Visibility generation and image reconstruction using SEPS Light

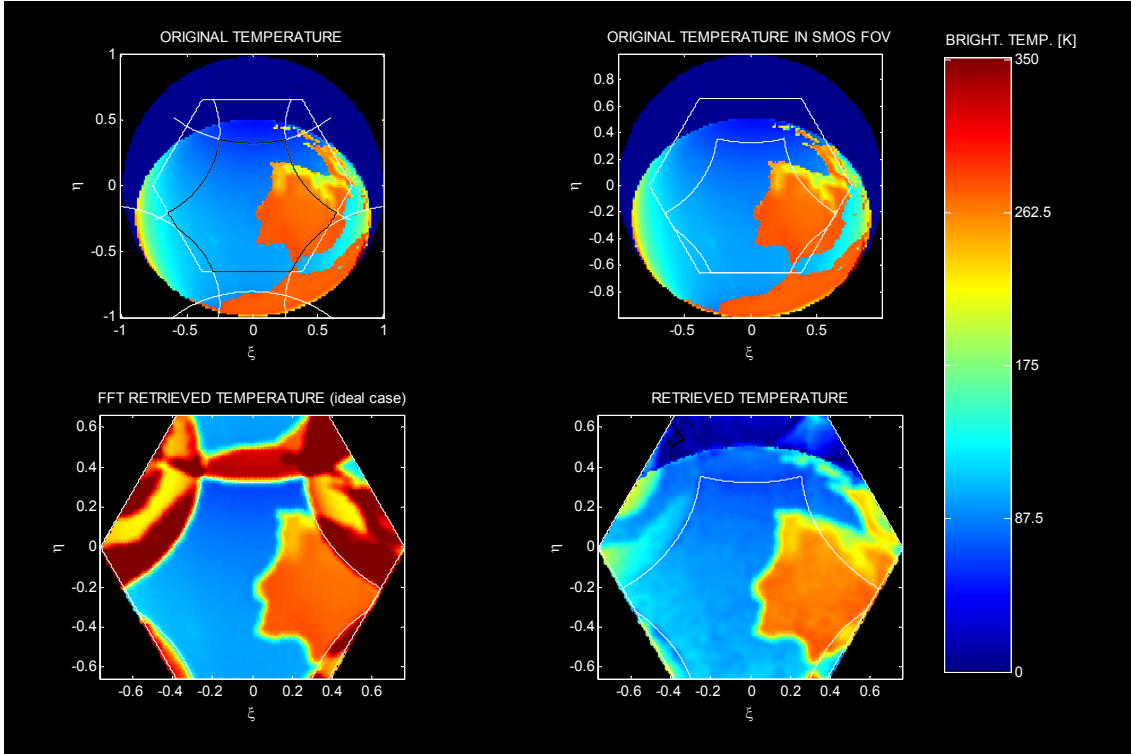


Fig. 22 X-pol. TB. Visibility generation and image reconstruction using SEPS Light

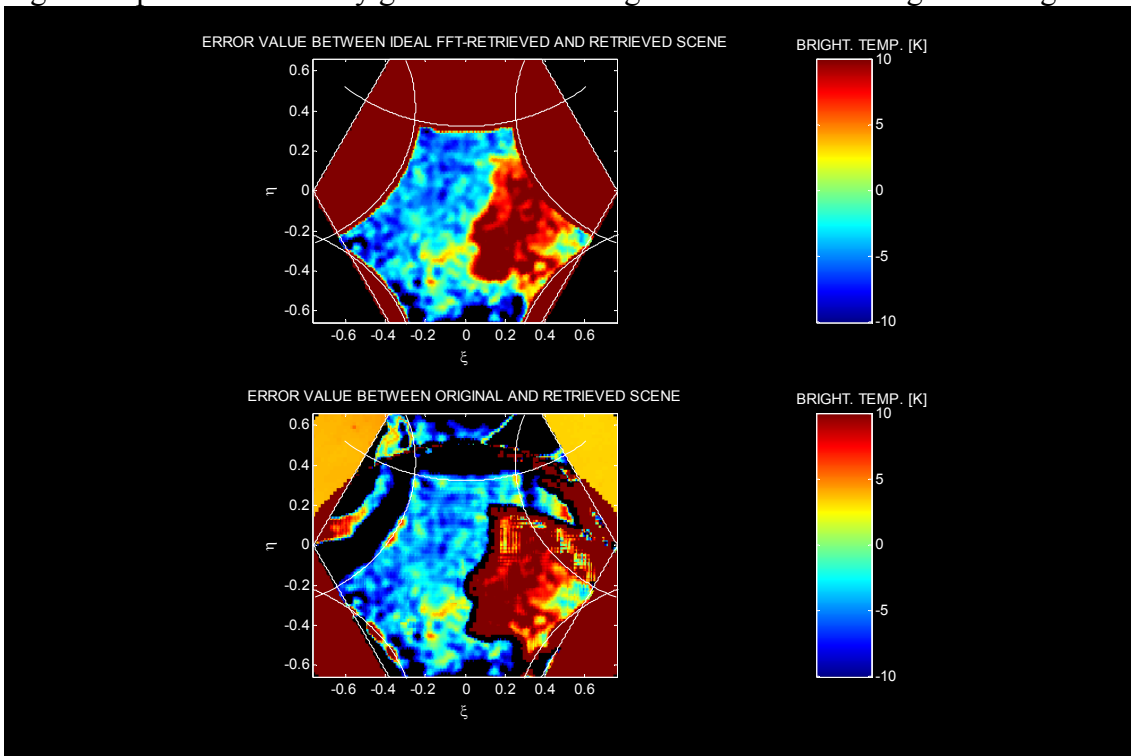


Fig. 23. X-pol. TB error. Visibility generation and image reconstruction using SEPS Light